Phytogenic Silver Nanoparticles as a Bioengineered Platform for Multifunctional Therapeutics: Synthesis, Characterization, and Biomedical Potential

Anam Ahsan *, George F Gao, Wen-Xia Tian *

Posted Date: 20 October 2025

doi: 10.20944/preprints202510.1499.v1

Keywords: green synthesis; silver nanoparticles; *Ricinus communis*; *Aloe barbadensis*; biomedical applications

 doi:10.20944/preprints202510.1499.v1

Article

Phytogenic Silver Nanoparticles as a Bioengineered Platform for Multifunctional Therapeutics: Synthesis, Characterization, and Biomedical Potential

Anam Ahsan [1,2,*], George F Gao [3] and Wen-Xia Tian [2,*]

[1] Centre for Pharmaceutical Innovation, University of South Australia, Adelaide, SA 5000, Australia
[2] College of Animal Science & Veterinary Medicine, Shanxi Agricultural University, Taigu 030801, China
[3] Institute of Microbiology, Chinese Academy of Sciences, Shijingshan 100043, Beijing, China
* Correspondence: anam.ahsan@mymail.unisa.edu.au (A.A.); wentiatian@126.com (W.T.)

Abstract

The green synthesis of silver nanoparticles (SNPs) using medicinal plants provides a sustainable and eco-friendly approach to nanoparticle production with promising biomedical potential. In this study, *Ricinus communis* and *Aloe barbadensis* aqueous leaf extracts were employed as reducing and stabilizing agents to synthesize *R. communis* SNPs (RcSNPs) and *A. barbadensis* SNPs (AbSNPs). The nanoparticles were characterized using ultraviolet–visible spectroscopy, dynamic light scattering, Fourier-transform infrared spectroscopy, scanning electron microscopy, transmission electron microscopy, thermogravimetric analysis, and differential scanning calorimetry to evaluate their physicochemical and thermal properties. RcSNPs and AbSNPs were predominantly spherical, with average sizes of 15–20 nm and 23–28 nm, respectively, and exhibited stability up to ~90 °C. Biological evaluations demonstrated potent antimicrobial, antioxidant, anti-inflammatory, anti-tyrosinase, anticoagulant, and cytotoxic activities. Notably, RcSNPs and AbSNPs induced apoptosis through mitochondrial pathway modulation and showed superior cytotoxicity compared to crude plant extracts and several previously reported SNPs. These findings indicate that phytochemical-mediated SNPs not only provide a green route of synthesis but also exhibit multifunctional bioactivities, which may support their potential applications as antimicrobial, antioxidant, depigmenting, and anticancer agents in biomedical and pharmaceutical fields.

Keywords: green synthesis; silver nanoparticles; *Ricinus communis*; *Aloe barbadensis*; biomedical applications

1. Introduction

Nanoscience has advanced rapidly, leading to the development of various nanoproducts that offer significant benefits to society [1]. Nanotechnology plays a crucial role in diverse fields such as biotherapy, pharmaceuticals, drug delivery, electronics, biotechnology, cosmetics, topical formulations (ointments and creams), nano-fertilizers, and water treatment [2]. Nanoparticles, defined as particulate matter with a diameter of less than 100 nm, exhibit unique properties that make them valuable in these applications [3,4]. Among these, silver nanoparticles (SNPs) have garnered widespread attention due to their exceptional electrical and thermal conductivity, as well as surface-enhanced Raman scattering [5–7]. Additionally, SNPs possess various biological activities, including antibacterial, antifungal, antioxidant, anti-inflammatory, anticancer effects, and potential use in gene therapy as non-viral carriers [8,9].

Several methods have been developed for the synthesis of SNPs, including chemical and electrochemical techniques. However, these approaches often encounter challenges during the purification stage due to the use of hazardous chemicals or the formation of toxic by-products, necessitating high energy input [10]. Moreover, controlling the size, shape, and achieving

 doi:10.20944/preprints202510.1499.v1

monodispersity of nanoparticles remain common challenges [10]. These limitations highlight the need for environmentally sustainable and safe synthesis methods. Consequently, green chemistry-based approaches have gained prominence in recent years [11,12].

Green synthesis involves the biological reduction of metal ions into nanoparticles using microorganisms or plant-derived extracts obtained from leaves, fruits, and seeds [13]. Plant extracts are rich in secondary metabolites such as alkaloids, terpenoids, flavonoids, enzymes, cyclic peptides, amino acids, proteins, polysaccharides, tannins, retinoic acid, ascorbic acid, polyphenols, and other compounds, which act as reducing agents, capping agents, and stabilizers during nanoparticle synthesis [14–16]. These compounds not only facilitate the synthesis process but also enhance the biological activity of the resulting nanoparticles. Furthermore, green synthesis offers advantages such as well-defined size and morphology, ease of scale-up, and high-yield production without surface contamination [12,17,18].

Numerous plants and plant parts have been utilized for the biosynthesis of SNPs, including *Diospyros lotus* [11], *Sida rhombifolia* [19], grape seeds [20], *Physalis angulata* [21], *Soymida febrifuga* [22], algae (*Parachlorella kessleri*) [23], chamomile (*Matricaria recutita*) [24], and *Ilex paraguariensis* [25]. The selection of plant sources often favors those that are readily available and renewable [26]. Factors such as extract concentration, metal salt concentration, temperature, pH, and reaction time significantly influence the rate of nanoparticle formation, yield, and physicochemical properties [12,27–29].

In this study, we aimed to synthesize optimized silver nanoparticles using the leaves of *Ricinus communis* and *Aloe barbadensis*, perform detailed optimization of synthesis parameters, and evaluate their therapeutic potential.

2. Materials and Methods

2.1. Materials

Silver nitrate, bovine serum albumin (BSA), and other chemicals were purchased from Sigma-Aldrich (USA). B16F10 murine melanoma and HepG2 human hepatocarcinoma cell lines were obtained from the Chinese Academy of Sciences Cell Bank (Shanghai, China). RPMI-1640, Dulbecco's Modified Eagle's Medium (DMEM), fetal bovine serum (FBS), and trypsin were supplied by Thermo Fisher Scientific (MA, USA). All other reagents were of analytical grade, and double-distilled water was used throughout.

2.2. Methods

2.2.1. Preparation of Plant Extracts

Fresh leaves of *R. communis* and *A. barbadensis* were collected from Shanxi Agricultural University, washed with running and double-distilled water, and air-dried at room temperature. Approximately 20 g of powdered *R. communis* leaves and sliced *A. barbadensis* leaves were separately boiled in 200 mL distilled water for 30 minutes. The extracts were cooled, filtered through Whatman No. 1 paper, and stored at 4 °C until further use.

2.2.2. Phytochemical Analysis

Qualitative screening of aqueous leaf extracts was performed to detect alkaloids, phenols, proteins, carbohydrates, glycosides, steroids, saponins, tannins, flavonoids, and terpenoids using standard procedures [30–32].

2.2.3. Total Phenolic Content (TPC) Estimation

TPC was determined using a modified Folin–Ciocalteu method [33]. Briefly, 100 µg/mL of plant extract or gallic acid standard was mixed with 0.5 mL Folin–Ciocalteu reagent, incubated in the dark

 doi:10.20944/preprints202510.1499.v1

for 10 minutes, followed by addition of 2.5 mL 20% sodium carbonate. After 1 hour in the dark, absorbance was measured at 765 nm using a UV–Vis spectrophotometer.

2.2.4. Biogenic Synthesis of Silver Nanoparticles (SNPs)

A 1 mM $AgNO_3$ solution (100 mL) was prepared. For *R. communis* silver nanoparticles (RcSNPs) or *A. barbadensis* silver nanoparticles (AbSNPs) synthesis, 1 mL of *R. communis* or *A. barbadensis* leaf extract was added dropwise to 9 mL $AgNO_3$ in separate flasks. The mixtures were shaken, incubated in the dark at room temperature, and a control without extract was maintained. SNP solutions were purified by repeated centrifugation (10,000 rpm, 15 min) and redispersed in deionized water three times, then freeze-dried for further characterization.

2.2.5. Optimization of SNP Synthesis

$AgNO_3$ concentrations (0.05–4 mM) and extract volumes (1–4 mL) were varied to optimize SNP synthesis. With optimized concentrations, reaction time (30 min–24 h), temperature (25–110 °C), and pH (2–13) were systematically evaluated. UV–Vis spectra were recorded at 300–800 nm, and all glassware was covered to prevent photo-degradation [34,35].

2.2.6. Visual Inspection

SNP formation was initially confirmed by observing a color change of the reaction mixtures over 24 hours.

2.2.7. UV–Visible Spectroscopy

Absorption spectra of SNPs were recorded using a Shimadzu UV-2600i spectrophotometer (300–800 nm) with 1 mL aliquots of diluted reaction mixtures at various time intervals.

2.2.8. Stability Study

Purified SNPs were stored in the dark at ambient conditions. Stability was monitored via UV–Vis spectroscopy (300–800 nm) over a period of up to 30 days.

2.2.9. Characterization of SNPs

DLS and Zeta Potential: Hydrodynamic size and surface charge were measured using a Brookhaven instrument. SNPs (5 mg) were dispersed in 5 mL water, sonicated, and measured at 689 nm, 90 °C, with three readings per sample.

FTIR Spectroscopy: FTIR spectra of leaf extracts and SNPs were obtained using KBr pellets on a Bruker Infra-red Affinity-1 (400–4000 cm^{-1}, 4 cm^{-1} resolution).

SEM Analysis: Morphology was visualized by SEM (JSM-5600, Tokyo, Japan) on thin films of SNPs prepared on carbon-coated copper grids.

TEM Analysis: Size and morphology were confirmed by TEM (JEOL, JEM-100 CX II) using SNP suspensions (1 μg/mL) on copper grids dried at 37 °C.

TGA and DSC: Thermal stability was assessed using a Hitachi thermal analyzer. Lyophilized SNPs (8.6 mg) were heated from 40–900 °C at 10 °C/min under N_2 flow (40 mL/min), with reference crucibles used for comparison.

2.2.10. Antimicrobial Activity

SNPs were tested against *S. aureus*, *E. coli*, *S. typhi*, *C. albicans*, and *A. niger*. Gentamicin and fluconazole were positive controls.

Agar Well Diffusion: Cultures were standardized to 0.5 McFarland (~1.5 × 10^8 CFU/mL). Mueller–Hinton agar (bacteria) or potato dextrose agar (fungi) plates were inoculated, and SNP

 doi:10.20944/preprints202510.1499.v1

solutions (50 µL, 50–100 µg/mL) were added to wells. Plates were incubated at 37 °C for 24 h, and zones of inhibition were measured [36].

2.2.11. Anticoagulant Activity

Blood (2 mL) from healthy volunteers (22–40 years) was incubated with 50 µg of *R. communis* Silver nanoparticles (RcSNPs) or *A. barbadensis* silver nanoparticles (AbSNPs) to assess anticoagulant potential. Controls contained blood without SNPs.

2.2.12. In Vitro Anti-Inflammatory Assays

Protein Denaturation: 500 µL BSA (1%) was mixed with 100 µL extract or SNPs (pH 6.3), incubated at 37 °C for 20 min, then heated at 55 °C for 20 min. Absorbance at 660 nm was measured; acetylsalicylic acid was the positive control [37]. The following equation estimated the inhibition (%) of protein denaturation:

$$\% \text{ inhibition} = \frac{\text{absorbance}_{\text{control}} - \text{absorbance}_{\text{sample}}}{\text{Absorbance}_{\text{control}}} \times 100 \quad (1)$$

Protease Inhibition: 100 µL extract/SNPs was mixed with 100 µL BSA, incubated 5 min, then 250 µL trypsin added. Supernatant absorbance at 210 nm measured protease inhibition [38].

2.2.13. In Vitro Antioxidant Assays

DPPH Assay: 250 µL 0.3 mM DPPH solution was mixed with 2.5 mL of extract/SNPs (10–100 µg/mL). BHT was positive control; absorbance measured for % inhibition [39].

H_2O_2 Scavenging: Extracts/SNPs (10–100 µg/mL) were mixed with 50 mL 5 mM H_2O_2, incubated 20 min, absorbance at 610 nm recorded [40].

Nitric Oxide Scavenging: Sodium nitroprusside (20 mM) generated NO, incubated with extract/SNPs (10–100 µg/mL) 60 min, nitrite measured via Griess reagent [41].

Reducing Power: Extracts/SNPs (10–100 µg/mL) were mixed with phosphate buffer and 1% potassium ferricyanide, incubated 50 °C, cooled, TCA added, centrifuged, supernatant mixed with ferric chloride, absorbance at 700 nm measured [42].

2.2.15. Tyrosinase Inhibition

SNPs were tested with L-tyrosine and mushroom tyrosinase in 50 mM potassium phosphate buffer (pH 6.8) at 30 °C. Pre-incubation 10 min, absorbance at 492 nm recorded, and % inhibition calculated [43].

2.2.16. In Vitro Cytotoxicity

Cell Culture: B16F10 and HepG2 cells were maintained at 37 °C, 5% CO_2, detached with 0.25% trypsin, and seeded at 3×10^3 cells/well in 96-well plates.

Cytotoxicity Evaluation: Cells treated with SNPs (0–100 µg/mL) for 24 h. MTT assay performed; formazan dissolved in DMSO, absorbance at 570 nm measured [44].

$$\text{Cell viability (\%)} = (OD_{\text{sample}}/OD_{\text{control}}) \times 100 \quad (2)$$

Here OD_{sample} denotes the absorbance of treated cells while $OD_{control}$ is the absorbance of untreated cells used as control.

2.2.17. Statistical Analysis

All experiments were performed in triplicate. Data are presented as mean ± SD and analyzed using one-way ANOVA with GraphPad Prism v5.

 doi:10.20944/preprints202510.1499.v1

3. Results

3.1. Phytochemical Analysis

Phytochemical screening of aqueous and methanol leaf extracts of *Ricinus communis and Aloe barbadensis* revealed the presence of various bioactive constituents. The results, summarized in Table 1, indicate that both plant extracts contain key biomolecules such as alkaloids, phenols, proteins, carbohydrates, glycosides, steroids, saponins, tannins, flavonoids, and terpenoids, which may contribute to their therapeutic potential.

Table 1. Phytochemical analysis of *Ricinus communis* and *Aloe barbadensis* leaf extracts.

Phytochemicals	**Aqueous extract**		**Methanolic extract**	
	Ricinus communis	*Aloe barbadensis*	*Ricinus communis*	*Aloe barbadensis*
Alkaloids	-	+	+	+
Steroids	-	-	+	+
Flavonoids	+	+	+	+
Terpenoids	+	-	+	+
Glycosides	+	-	-	-
Phenols	-	+	+	+
Tannins	+	+	+	-
Saponins	+	-	+	+
Reducing sugars	+	+	+	+

3.2. Visual Inspection

The synthesis of silver nanoparticles (SNPs) can be initially indicated by a distinct color change in the reaction mixture, which occurs due to the excitation of surface plasmon resonance (SPR) of SNPs [45,46]. Typically, the solution transitions from colorless to yellow, pale yellow, yellowish-brown, and eventually to dark brown. In the present study, a progressive change in color from yellowish to light brown, and finally to dark brown, was observed upon addition of the plant extract to silver nitrate solution, confirming the formation of SNPs (Figure 1).

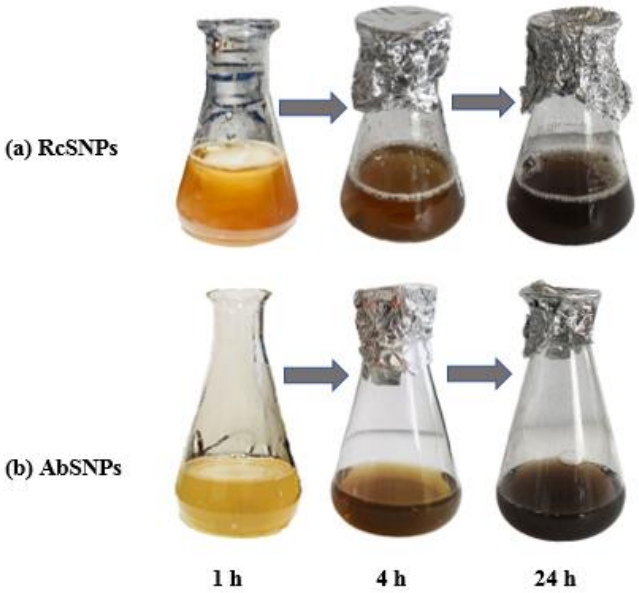

 doi:10.20944/preprints202510.1499.v1

Figure 1. Color change in the reaction mixture of silver nanoparticles synthesized from *Ricinus communis* (RcSNPs, a) and *Aloe barbadensis* (AbSNPs, b) over time (1 h, 4 h, and 24 h).

3.3. UV-Visible Spectroscopy

UV–visible (UV–vis) spectroscopy is a simple and widely used technique for monitoring the synthesis of silver nanoparticles (SNPs) [47]. In this study, reactions were carried out at room temperature. The characteristic surface plasmon resonance (SPR) bands observed near 435 nm for *R. communis* and 442 nm for *A. barbadensis* confirmed the reduction of Ag^+ ions to metallic silver. To optimize the synthesis, key parameters including $AgNO_3$ concentration, extract concentration, reaction time, temperature, and pH were systematically varied, as these factors strongly influence nanoparticle formation [28].

3.3.1. Effect of $AgNO_3$ Concentration

SNPs were synthesized using varying concentrations of $AgNO_3$ (0.5–4 mM), while maintaining the extract concentration at 1 mL under constant reaction conditions. No SPR band was detected at low $AgNO_3$ concentrations; however, distinct peaks were observed at 435 nm for 1 mM $AgNO_3$ with *R. communis* extract, and at 442 nm for 2 mM $AgNO_3$ with *A. barbadensis* extract. Increasing $AgNO_3$ concentration led to higher peak intensity and peak broadening, indicating an increase in SNPs concentration and particle aggregation (Figure 2a, f) [40]. Based on these results, the optimal $AgNO_3$ concentrations were set at 1 mM for *R. communis* and 2 mM for *A. barbadensis* for subsequent experiments.

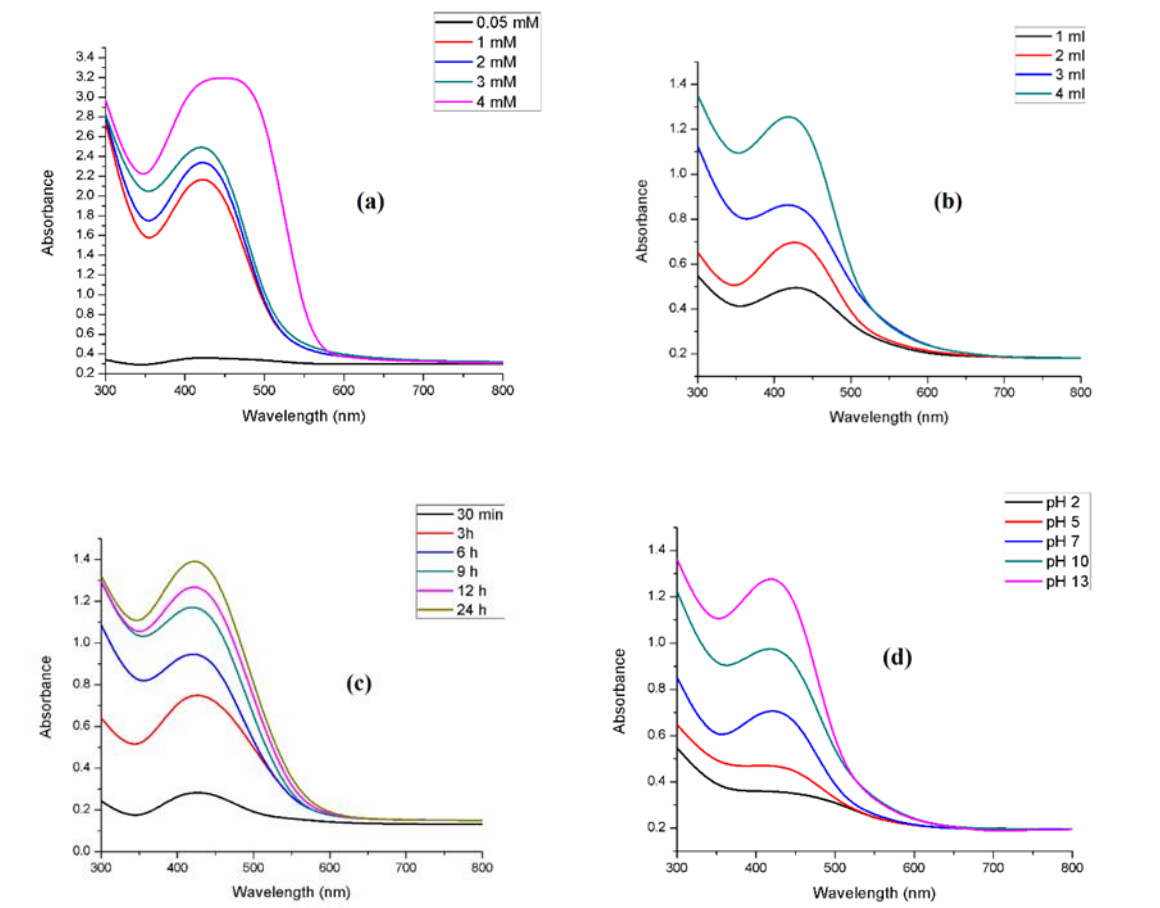

 doi:10.20944/preprints202510.1499.v1

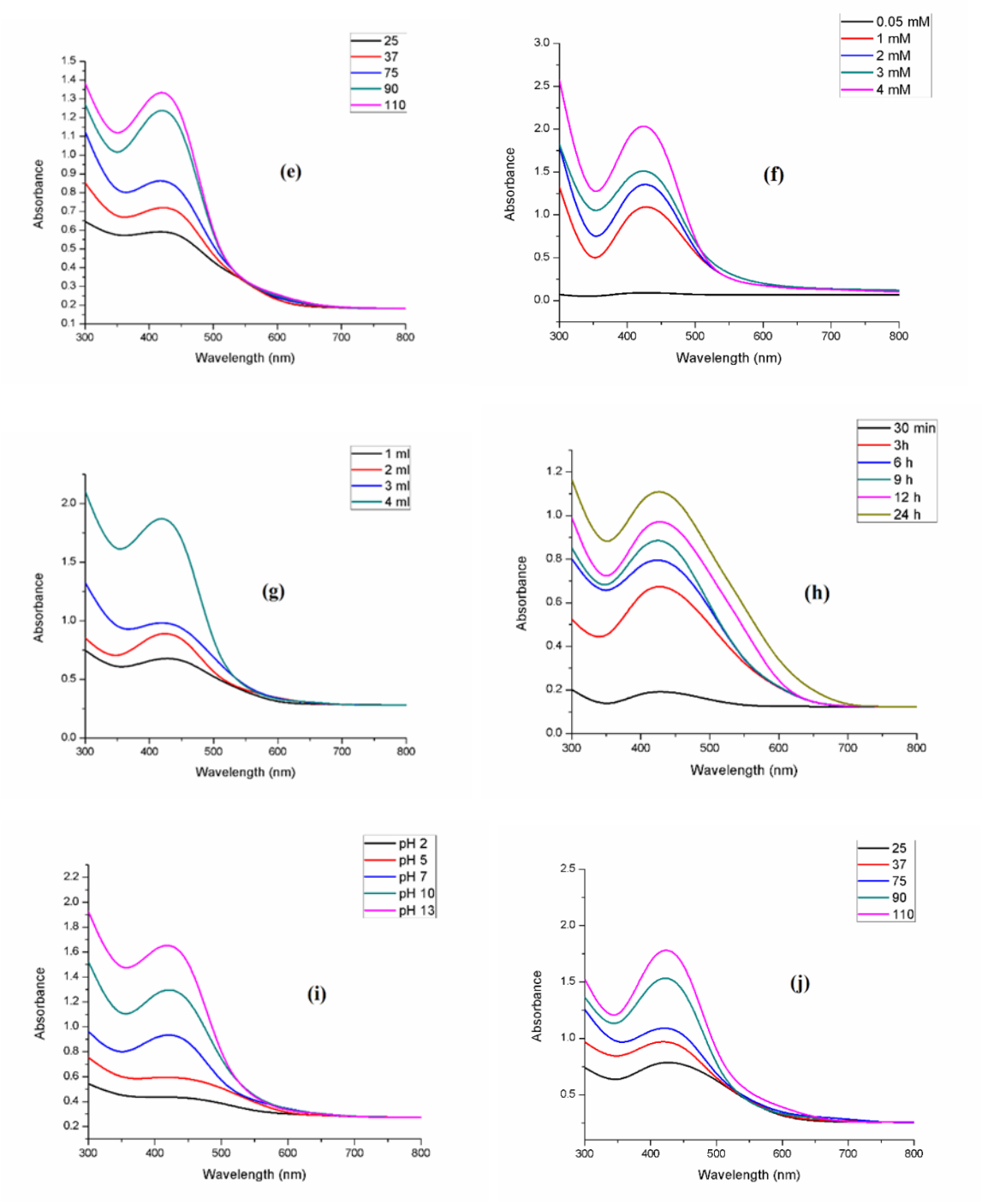

Figure 2. UV–visible spectra of silver nanoparticles synthesized from *Ricinus communis* (RcSNPs) and *Aloe barbadensis* (AbSNPs) showing the effects of varying parameters: $AgNO_3$ concentration (a, f), leaf extract concentration (b, g), reaction time (c, h), pH (d, i), and temperature (e, j). Data represent mean ± SD (n = 3).

3.3.2. Effect of Leaf Extract Concentration

Extract concentration also influenced nanoparticle properties. Optimization was performed by fixing $AgNO_3$ concentration and varying extract volume (1–4 mL). With increasing extract concentration, the SPR bands became narrower, suggesting improved monodispersity of SNPs (Figure 2b, g). An extract volume of 1 mL was determined to be optimal for further experiments.

3.3.3. Effect of Reaction Time

 doi:10.20944/preprints202510.1499.v1

Reaction time significantly affected SNP formation and stability. At the initial stage, no SPR peak appeared immediately after mixing silver nitrate with plant extracts. After 1 h, characteristic SPR bands at 435 nm (*R. communis*) and 442 nm (*A. barbadensis*) emerged, with peak intensity increasing over time. Maximum absorbance was recorded at 6 h for *R. communis* and 9 h for *A. barbadensis* (Figure 2c, h). Beyond these times, peak broadening occurred, likely due to agglomeration or increased particle size. Therefore, 6 h and 9 h were selected as the optimized reaction times for *R. communis* and *A. barbadensis*, respectively.

3.3.4. Effect of pH

pH had a notable influence on the morphology and stability of SNPs. Higher pH values enhanced the reduction of Ag^+ ions, resulting in stronger absorbance and improved stability of the nanoparticles (Figure 2d, i).

3.3.5. Effect of Temperature

Temperature variations also affected SNP synthesis. Although different temperatures were tested, room temperature was found to be optimal, producing small, spherical SNPs with a sharp and distinct single SPR band at shorter wavelengths (Figure 2e, j).

3.4. Stability of Synthesized SNPs

The stability of biosynthesized SNPs was evaluated by monitoring their UV–vis spectra over time. As shown in Figure 3a, b, prolonged storage led to a gradual decrease in absorbance intensity and band broadening, indicating possible agglomeration or partial release of metallic ions. Importantly, the SPR band position remained unchanged even after 30 days, suggesting that the nanoparticles retained their structural integrity [48]. In addition, reproducibility was confirmed by synthesizing SNPs in triplicate over a period of six months. The spectra remained consistent, demonstrating that *R. communis* and *A. barbadensis* extract-mediated SNPs possess excellent stability and dispersity.

 doi:10.20944/preprints202510.1499.v1

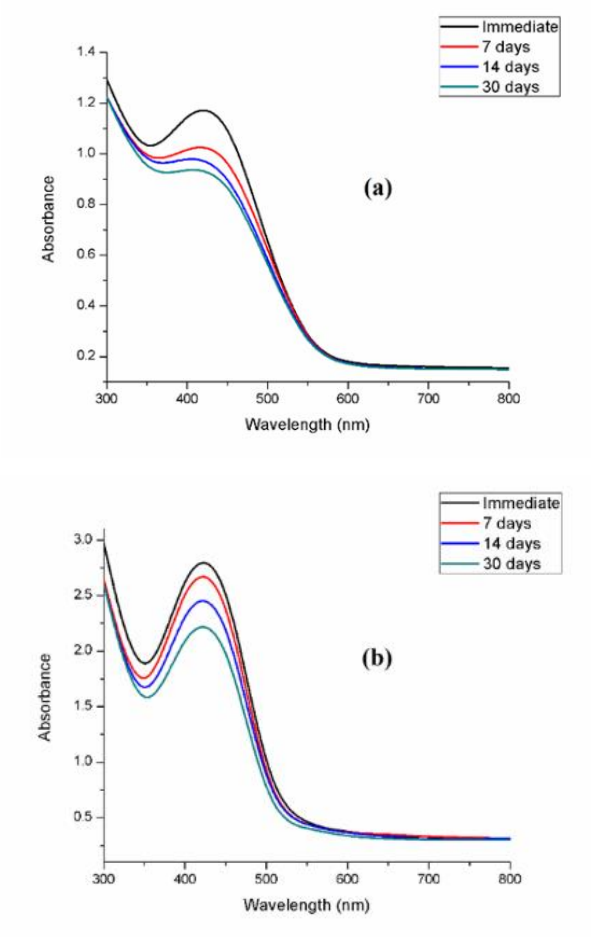

Figure 3. Stability studies of silver nanoparticles synthesized from *Ricinus communis* (RcSNPs, a) and *Aloe barbadensis* (AbSNPs, b) over a one-month period. Data represent mean ± SD (n = 3).

3.5. Dynamic Light Scattering (DLS) and Zeta Potential (ZP) Analysis

Dynamic light scattering (DLS) is a widely used technique for determining nanoparticle size distribution at the nanometer scale [49]. The DLS profiles of biogenic SNPs are presented in Figure 4a, b. Under optimized conditions, the average hydrodynamic diameter of RcSNPs and AbSNPs was 93.65 ± 1.55 nm and 126.09 ± 0.13 nm, respectively. The corresponding polydispersity index (PDI) values were 0.287 ± 0.002 and 0.130 ± 0.019, indicating narrow size distributions. The zeta potential (ZP) values were −67.09 mV (RcSNPs) and −83.42 mV (AbSNPs), confirming strong surface charge and excellent colloidal stability. These findings are consistent with the UV–vis analysis results.

 doi:10.20944/preprints202510.1499.v1

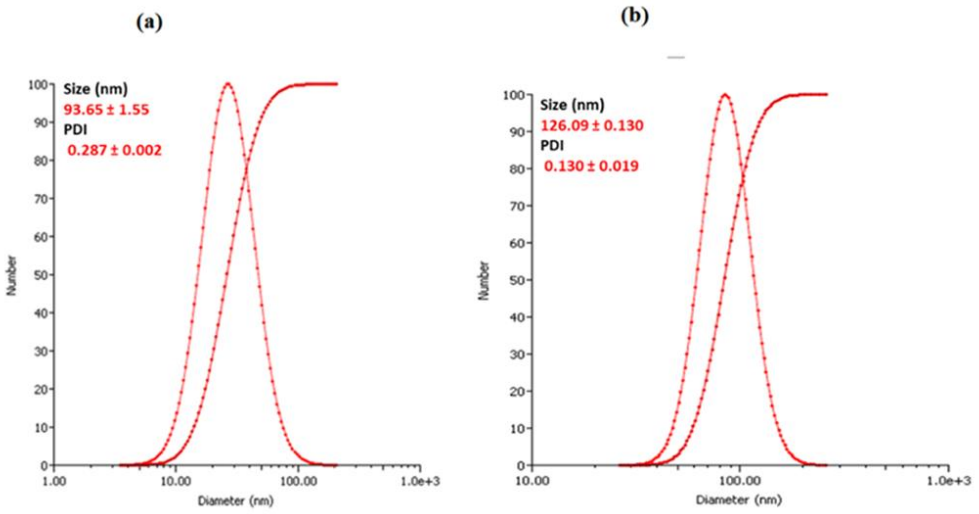

Figure 4. Dynamic light scattering (DLS) size distribution histograms of silver nanoparticles synthesized from *Ricinus communis* (RcSNPs, a) and *Aloe barbadensis* (AbSNPs, b). Data represent mean ± SD (n = 3).

3.6. Fourier Transform Infrared (FTIR) Spectroscopy

Fourier transform infrared (FTIR) spectroscopy was employed to investigate the surface chemistry of SNPs and to identify biomolecules responsible for reducing Ag^{+} ions and stabilizing the nanoparticles [50]. The FTIR spectra of both plant extracts and their corresponding SNPs were compared to identify characteristic peaks and spectral shifts.

For RcSNPs, prominent absorption bands were observed at 3326 cm^{-1} and 1720 cm^{-1}, while AbSNPs exhibited bands at 3576 cm^{-1} and 1850 cm^{-1} (Figure 5). The bands at 3326 cm^{-1} (RcSNPs) and 3576 cm^{-1} (AbSNPs) correspond to –OH stretching vibrations, whereas the bands at 1720 cm^{-1} and 1850 cm^{-1} are attributed to N–H stretching of amine groups, indicating the capping of SNPs by these functional groups. Additionally, lower intensity bands at 2105 cm^{-1} (RcSNPs) and 2157 cm^{-1} (AbSNPs) were detected, corresponding to carbonyl (C=O) stretching.

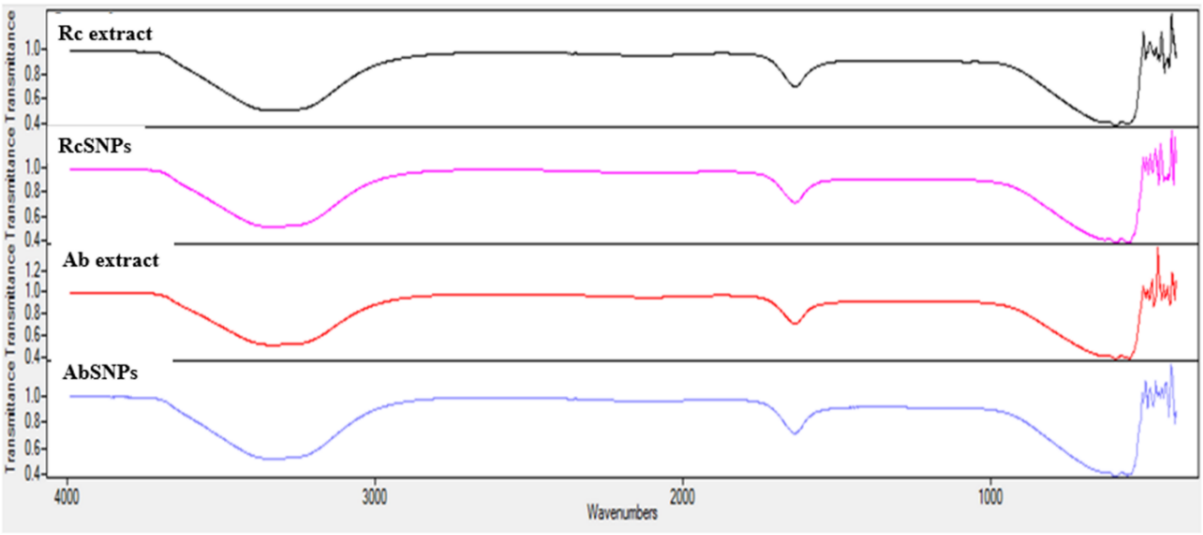

Figure 5. Fourier transform infrared (FTIR) spectra of *Ricinus communis* and *Aloe barbadensis* leaf extracts, and their corresponding silver nanoparticles (RcSNPs and AbSNPs).

3.7. Scanning Electron Microscopy (SEM) Analysis

 doi:10.20944/preprints202510.1499.v1

Scanning electron microscopy (SEM) was used to examine the morphology and size of the biosynthesized SNPs. The micrographs revealed nanoparticles with spherical, cubic, triangular, and rectangular shapes, distributed relatively evenly. Some degree of agglomeration was observed, likely due to the limited stabilization provided by weak capping agents [51]. The agglomerated particle sizes ranged from 256–272 nm for RcSNPs and 263–278 nm for AbSNPs, while the average particle sizes were estimated to be 68 nm (RcSNPs) and 74 nm (AbSNPs) (Figure 6a, b).

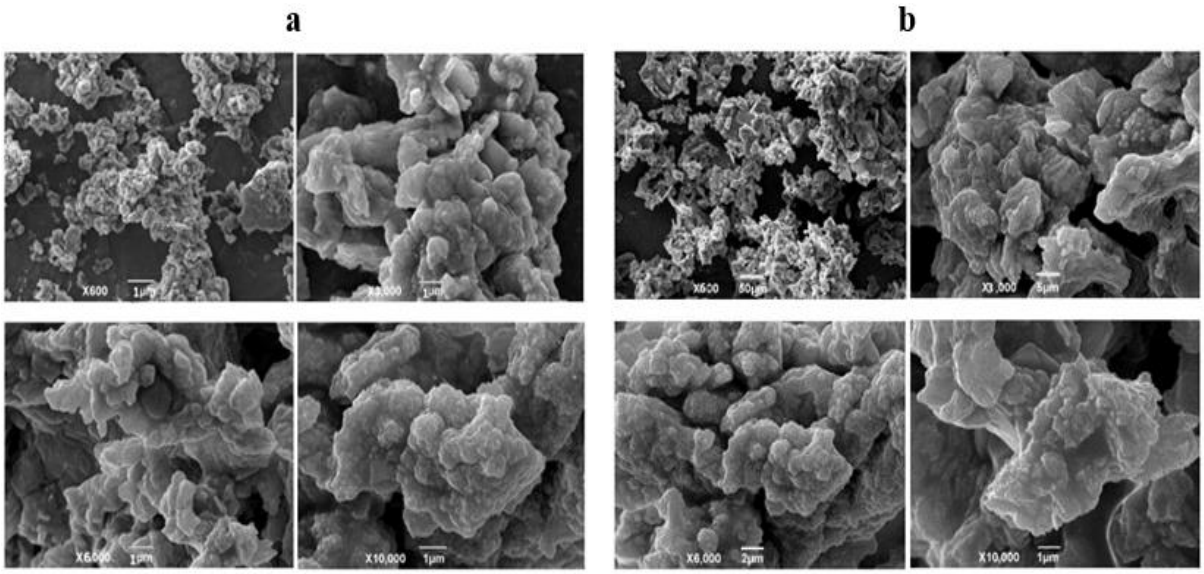

Figure 6. Scanning electron microscopy (SEM) images of silver nanoparticles synthesized from *Ricinus communis* (RcSNPs, a) and *Aloe barbadensis* (AbSNPs, b) at different magnifications (×600, ×3,000, ×6,000, ×10,000).

3.8. Transmission Electron Microscopy (TEM) Analysis

Transmission electron microscopy (TEM) provided further insights into the morphology and size of the biosynthesized SNPs (Figure 7a–d). The images revealed that most nanoparticles were spherical, consistent with the observations from UV–vis and SEM analyses. Particle size measurements performed using ImageJ software indicated sizes of 15–20 nm for RcSNPs and 23–28 nm for AbSNPs.

 doi:10.20944/preprints202510.1499.v1

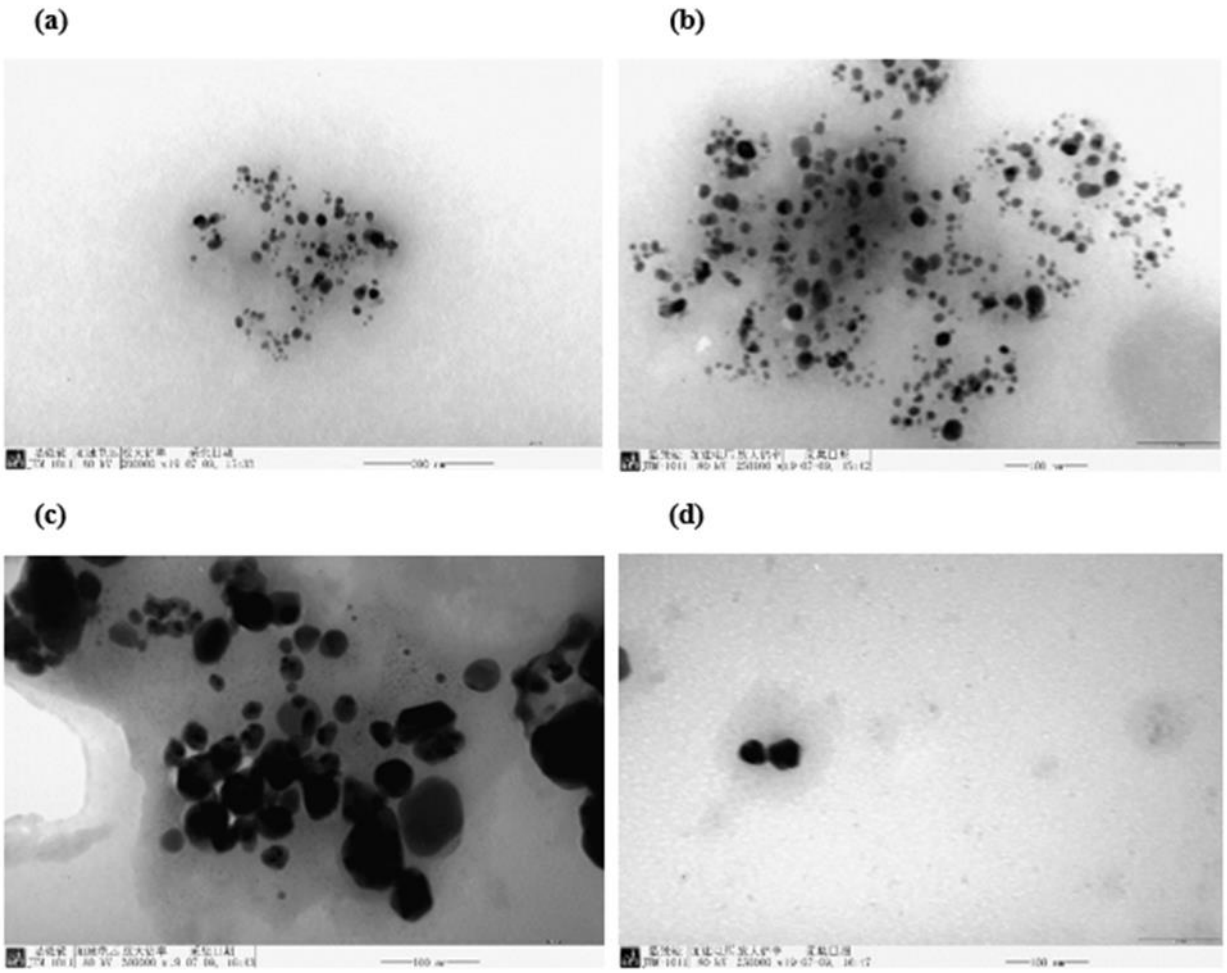

Figure 7. Transmission electron microscopy (TEM) images of silver nanoparticles synthesized from *Ricinus communis* (RcSNPs, a, b) and *Aloe barbadensis* (AbSNPs, c, d) at different magnifications.

3.9. Thermogravimetric Analysis (TGA) and Differential Scanning Calorimetry (DSC)

Thermogravimetric analysis (TGA) was performed to evaluate the thermal stability of the biosynthesized SNPs. The results indicated that RcSNPs began to degrade at approximately 200 °C, while AbSNPs showed initial degradation at 240 °C. A gradual weight loss was observed up to 800 °C (Figure 8a, b). Differential scanning calorimetry (DSC) revealed endothermic peaks at 190 °C for RcSNPs and 220 °C for AbSNPs, corresponding to thermal transitions of the nanoparticles (Figure 8a, b).

 doi:10.20944/preprints202510.1499.v1

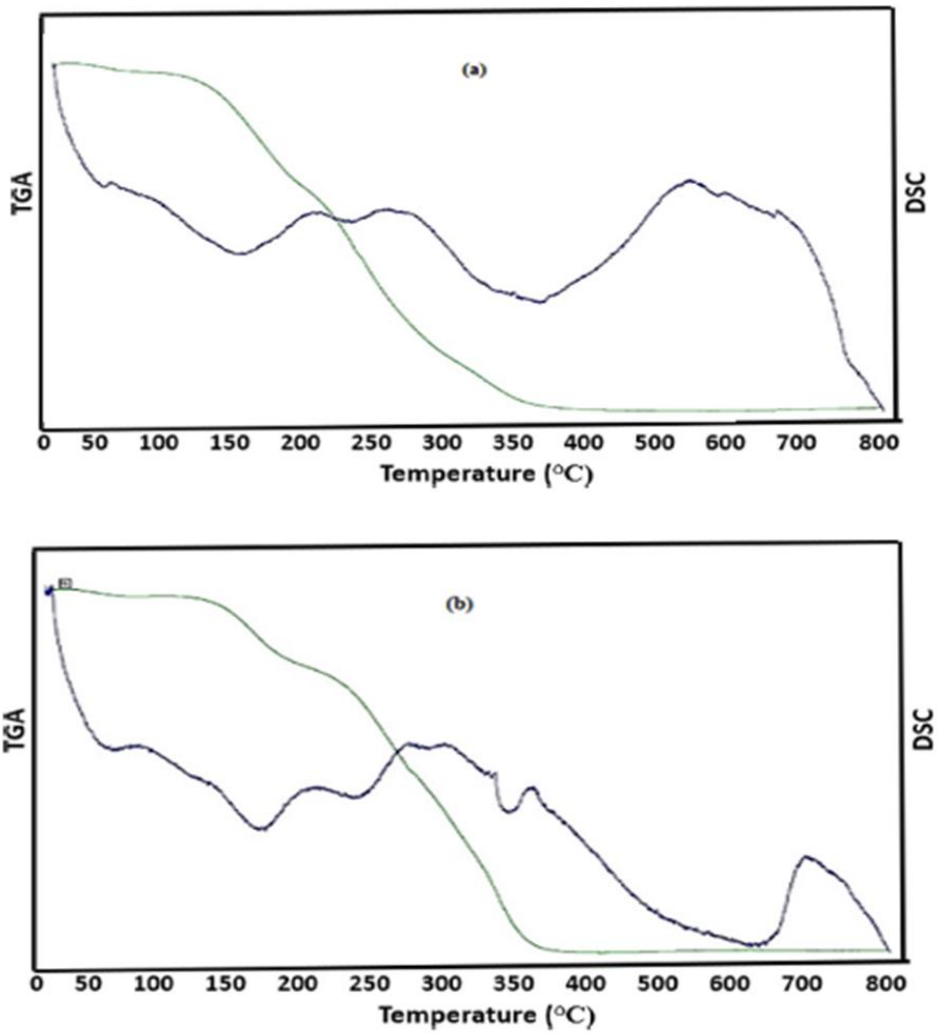

Figure 8. Thermogravimetric (TGA) and differential scanning calorimetry (DSC) thermograms of silver nanoparticles synthesized from *Ricinus communis* (RcSNPs, a) and *Aloe barbadensis* (AbSNPs, b).

3.10. Antimicrobial Activity of Biogenic SNPs

The antimicrobial potential of RcSNPs and AbSNPs was evaluated against selected bacterial and fungal pathogens, and their efficacy was quantified by measuring the zones of inhibition (mm) (Figure 9, 10; Table 2).

 doi:10.20944/preprints202510.1499.v1

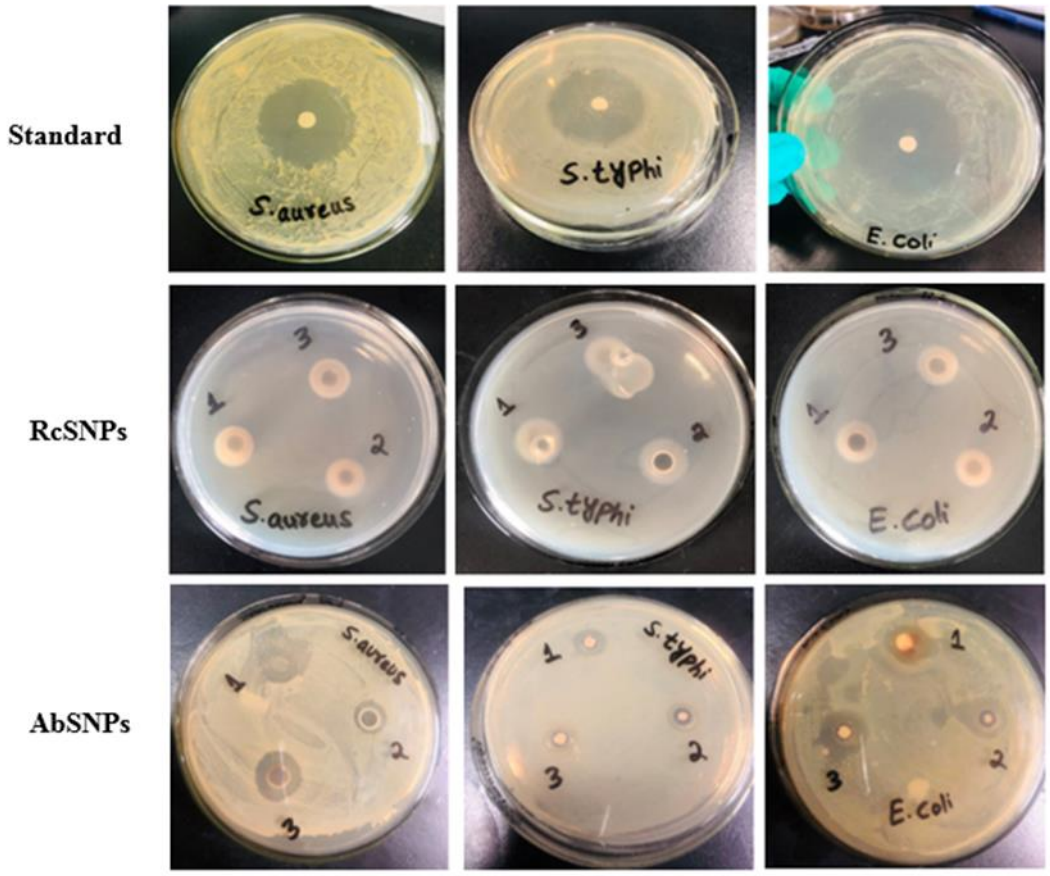

Figure 9. Antibacterial activity of silver nanoparticles synthesized from *Ricinus communis* (RcSNPs) and *Aloe barbadensis* (AbSNPs) against pathogenic bacterial strains. Treatments: leaf extract (1), 50 µL SNPs (2), 100 µL SNPs (3). Data represent mean ± SD (n = 3).

RcSNPs exhibited zones of inhibition of 22.3 ± 0.75 mm against *C. albicans* and 20.2 ± 0.93 mm against *S. aureus*, followed by 18.4 ± 0.65 mm, 19.3 ± 0.52 mm, and 21.4 ± 0.70 mm against *A. niger*, *S. typhi*, and *E. coli*, respectively. For AbSNPs, the corresponding zones were 21.8 ± 0.43 mm and 20.3 ± 0.051 mm against *A. niger* and *S. aureus*, and 24.3 ± 0.54 mm, 18.6 ± 0.07 mm, and 17.3 ± 0.049 mm against *C. albicans*, *S. typhi*, and *E. coli*, respectively (Figure 9,10).

 doi:10.20944/preprints202510.1499.v1

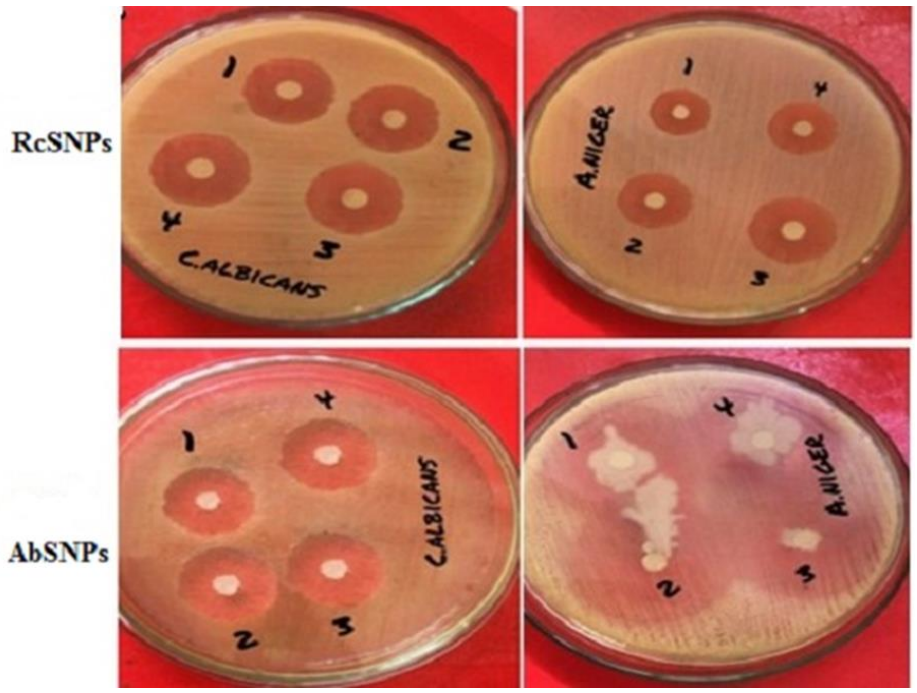

Figure 10. Antifungal activity of silver nanoparticles synthesized from *Ricinus communis* (RcSNPs) and *Aloe barbadensis* (AbSNPs) against pathogenic fungal strains. Treatments: leaf extract (1), fluconazole (2), 50 µL SNPs (3), 100 µL SNPs (4). Data represent mean ± SD (n = 3).

Both SNPs demonstrated the highest antibacterial activity against *S. aureus*, followed by *S. typhi* and *E. coli*. When compared to the aqueous leaf extracts of *R. communis* and *A. barbadensis*, RcSNPs showed enhanced antibacterial activity against *S. typhi*, whereas AbSNPs were more effective against *E. coli*. Regarding antifungal activity, RcSNPs exhibited superior inhibition of *C. albicans*, while AbSNPs were more active against *A. niger*. Notably, the antifungal activity of both SNPs exceeded that of the standard antifungal agent, fluconazole, highlighting their strong potential as antimicrobial agents.

Table 2. Zones of inhibition (mm) of RcSNPs, AbSNPs, standard antimicrobial drugs, and leaf extracts of *Ricinus communis* (Rc) and *Aloe barbadensis* (Ab) against pathogenic bacterial and fungal strains.

Microorganisms		RcSNPs		AbSNPs		Standard		Control	
		50 µL	100 µL	50 µL	100 µL	Gentamycin	Fluconazole	Rc extract	Ab extract
Bacteria	*S. aureus*	18.32±0.34	20.2±0.23	17.2±0.082	20.3±0.051	25.2±0.34	-	12.3±0.42	10.4±0.45
	S. typhi	18.1±0.72	19.3±0.52	14.5±0.067	18.6±0.070	27.8±0.54	-	14.6±0.36	8.6±0.58
	E. coli	17.6±0.93	18.4±0.65	16.1±0.047	17.3±0.049	23.4±0.65	-	11.2±0.71	11.7±0.32
Fungi	*C. albicans*	20.1±0.65	22.3±0.75	17.25±0.25	20.5±0.54	-	22.8±0.74	10.7±0.93	13.6±0.15
	A. niger	19.4±0.67	21.4±0.70	22.5±0.32	24.3±0.43	-	23.21±0.75	9.8±0.23	17.1±0.75

Experiments were performed in triplicates and the values are expressed as mean+ SD.

3.11. Anticoagulant Activity

 doi:10.20944/preprints202510.1499.v1

The anticoagulant potential of RcSNPs and AbSNPs was assessed by adding defined concentrations of the nanoparticles to coagulated blood. Control tubes without SNPs are shown in Figure 11a, c, while the anticoagulant effect of RcSNPs and AbSNPs is illustrated in Figure 11b, d. As observed, even a small quantity of SNPs effectively inhibited blood coagulation, indicating their promising anticoagulant activity.

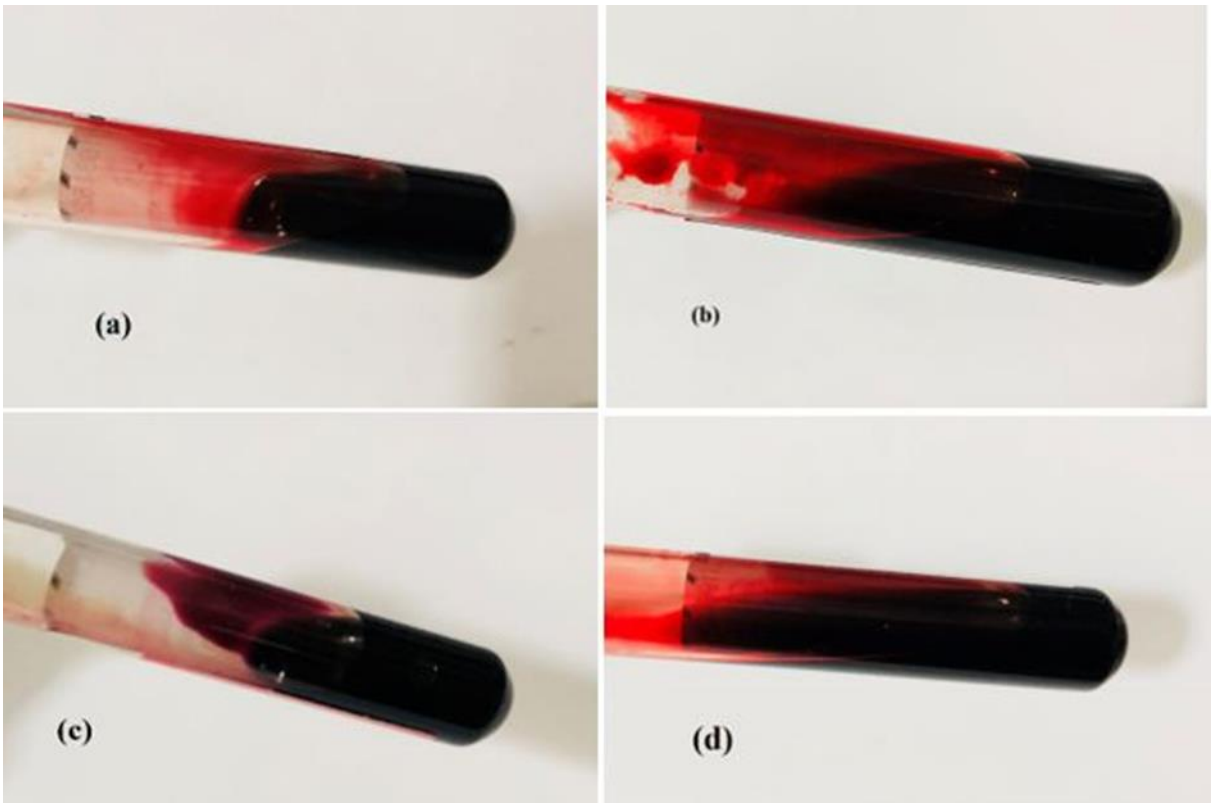

Figure 11. Anticoagulant effect of silver nanoparticles synthesized from *Ricinus communis* (RcSNPs, b) and *Aloe barbadensis* (AbSNPs, d). Control tubes without any anticoagulant are shown in (a, c). Data represent mean ± SD (n = 3).

3.12. In Vitro Anti-Inflammatory Assay

The anti-inflammatory potential of *R. communis* and *A. barbadensis* extracts and their corresponding SNPs was evaluated using the heat-induced albumin denaturation method. The plant extracts exhibited 67.45 ± 1.7% (*R. communis*) and 66.03 ± 1.8% (*A. barbadensis*) inhibition, whereas RcSNPs and AbSNPs showed significantly higher activity at 90.67 ± 1.7% and 89.79 ± 1.7%, respectively. Acetylsalicylic acid was used as the standard anti-inflammatory agent (Figure 12a). A concentration-dependent increase in inhibition was observed for both extracts and SNPs.

Furthermore, the extracts and SNPs demonstrated notable antiprotease activity. The standard drug, acetylsalicylic acid, exhibited the highest protease inhibitory effect (95.37 ± 1.3%). R. communis and *A. barbadensis* extracts showed 65.45 ± 1.6% and 63.03 ± 1.7% inhibition, respectively, whereas RcSNPs and AbSNPs displayed enhanced activity at 89.67 ± 1.4% and 87.79 ± 1.3%, respectively (Figure 12b).

 doi:10.20944/preprints202510.1499.v1

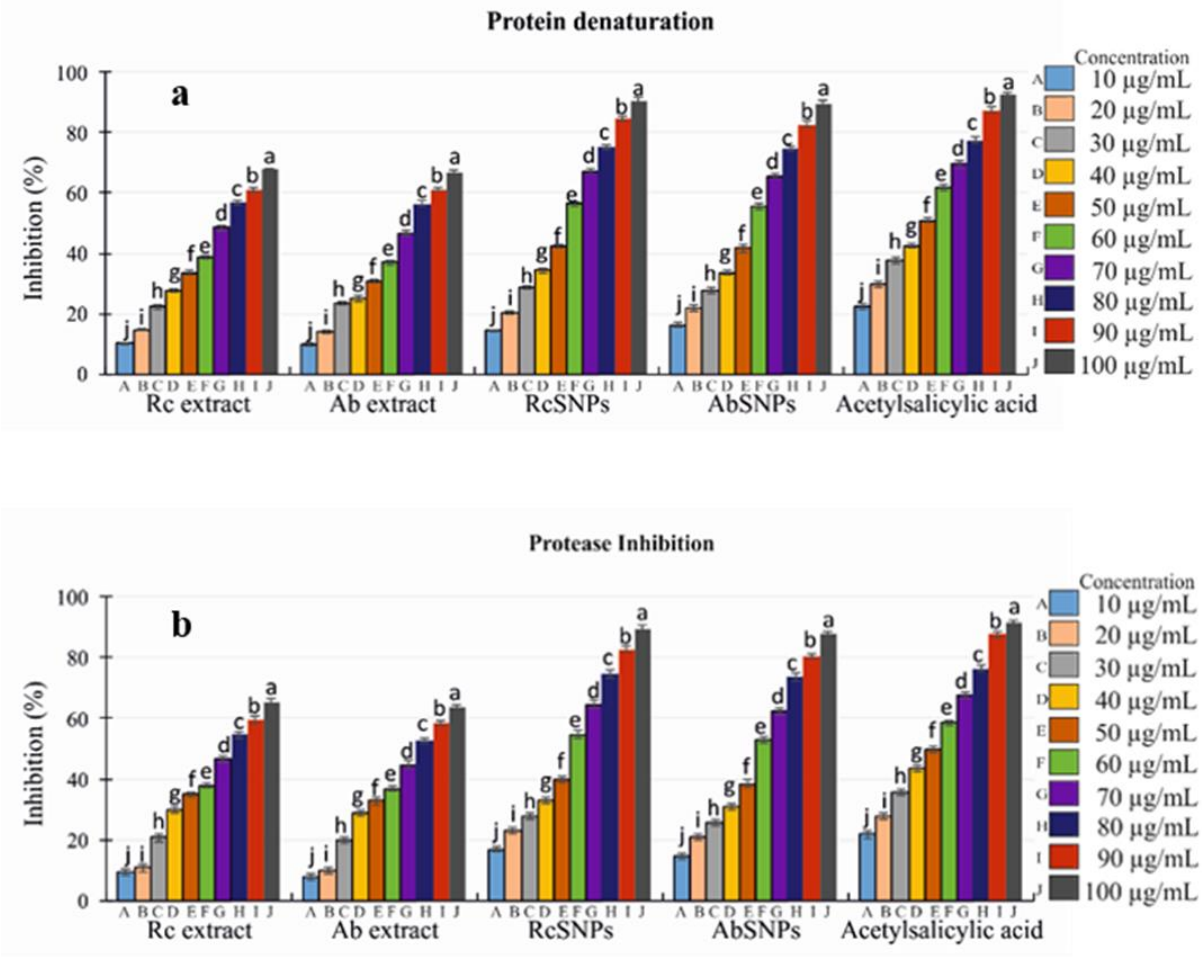

Figure 12. In vitro anti-inflammatory activity of *Ricinus communis* (Rc) and *Aloe barbadensis* (Ab) extracts and their corresponding SNPs. (a) Heat-induced protein denaturation; (b) Protease inhibition. Values with different superscripts (a–j) within the same variable are significantly different ($P < 0.05$).

3.13. In Vitro Antioxidant Assay

Free radicals are implicated in numerous human diseases, including arthritis, atherosclerosis, reperfusion injury, ischemia, central nervous system damage, gastritis, AIDS, and cancer. Recently, natural antioxidants have gained considerable attention due to their potential health benefits [51]. The antioxidant potential of *Ricinus communis* (Rc) and *Aloe barbadensis* (Ab) extracts and their corresponding SNPs was evaluated using DPPH, hydrogen peroxide (H_2O_2), nitric oxide (NO) scavenging, and reducing power assays.

In the DPPH assay, RcSNPs and AbSNPs demonstrated significant, concentration-dependent radical scavenging activity, with increasing inhibition observed at higher concentrations (10–100 µg/mL) (Figure 13a). Similarly, H_2O_2 scavenging activity was assessed spectrophotometrically, and RcSNPs, AbSNPs, and ascorbic acid exhibited 90.57 ± 0.9%, 89.02 ± 0.7%, and 92.05 ± 0.4% inhibition at 100 µg/mL, respectively (Figure 13b). H_2O_2 scavenging activity was slightly lower than DPPH scavenging for both SNPs, suggesting differential efficacy against specific reactive species.

 doi:10.20944/preprints202510.1499.v1

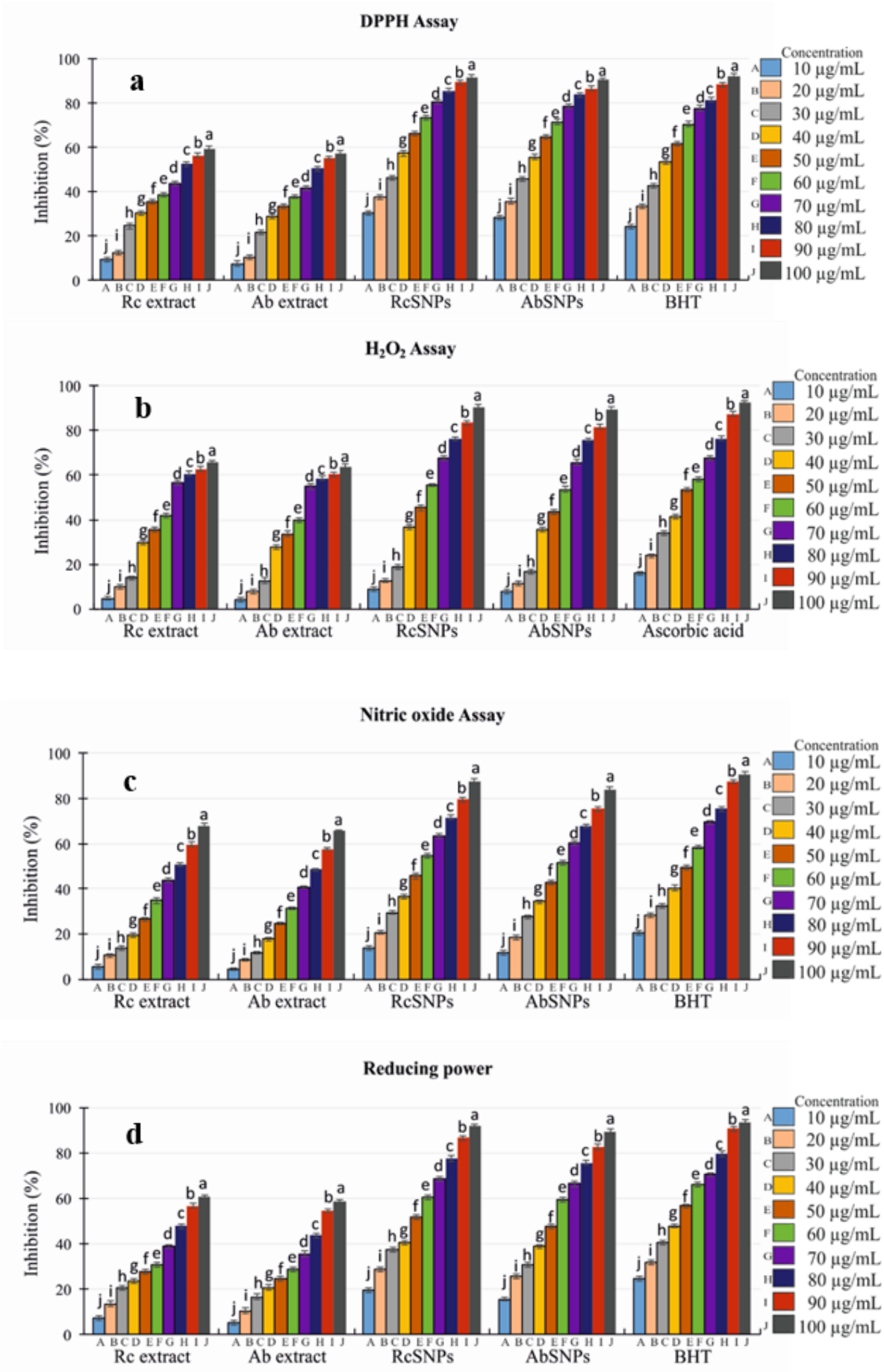

 doi:10.20944/preprints202510.1499.v1

Figure 13. In vitro antioxidant activity of *Ricinus communis* (Rc) and *Aloe barbadensis* (Ab) extracts and their corresponding SNPs. (a) DPPH assay; (b) H_2O_2 scavenging assay; (c) NO scavenging assay; (d) Reducing power assay. Values with different superscripts (a–j) within the same variable are significantly different ($P < 0.05$).

Biogenic RcSNPs and AbSNPs also exhibited NO scavenging activity in a dose-dependent manner, achieving 87.41 ± 1.8% and 83.87 ± 1.7% inhibition at 100 µg/mL, respectively, slightly lower than the standard BHT (90.83 ± 1.8%) (Figure 13c). The reducing power of the SNPs similarly increased with concentration, with maximum activities of 91.41 ± 1.6% (RcSNPs) and 89.08 ± 1.7% (AbSNPs), comparable to BHT (93.76 ± 1.7%) (Figure 13d).

Overall, these results indicate that both RcSNPs and AbSNPs possess strong, concentration-dependent antioxidant potential, comparable to standard antioxidant agents, highlighting their promising therapeutic value.

3.14. Tyrosinase Inhibition Activity

RcSNPs and AbSNPs exhibited potent tyrosinase inhibitory activity, with inhibition percentages of 97.98 ± 1.5% and 98.43 ± 1.5%, respectively (Table 3). These results indicate that both biogenic SNPs are highly effective in inhibiting tyrosinase, suggesting their potential applications in skin-whitening and anti-melanogenic formulations.

Table 3. Tyrosinase inhibitory activity (%) of silver nanoparticles synthesized from Ricinus communis (RcSNPs) and Aloe barbadensis (AbSNPs). Values represent mean ± SD (n = 3).

Testing material	Tyrosinase inhibition (%)
RcSNPs	96.77±1.09
AbSNPs	97.72±0.75
Ascorbic acid	99.23± 0.68

3.15. In Vitro Cytotoxicity Evaluation

Given the diverse biological applications of silver nanoparticles, the anticancer potential of RcSNPs and AbSNPs was evaluated using the MTT assay [52,53]. B16F10 and HepG2 cells were treated with varying concentrations of biogenic RcSNPs and AbSNPs (0–100 µg/mL) for 24 and 48 hours.

Both RcSNPs and AbSNPs exhibited significant, dose-dependent cytotoxic effects against B16F10 and HepG2 cells (Figure 14a–d). The IC_{50} values at 24 hours were 10 µg/mL for RcSNPs and 12 µg/mL for AbSNPs. Cytotoxicity increased further after 48 hours of incubation, indicating a time-dependent enhancement of their anticancer activity. These results demonstrate the promising therapeutic potential of RcSNPs and AbSNPs as cytotoxic agents against melanoma and hepatocellular carcinoma cell lines.

 doi:10.20944/preprints202510.1499.v1

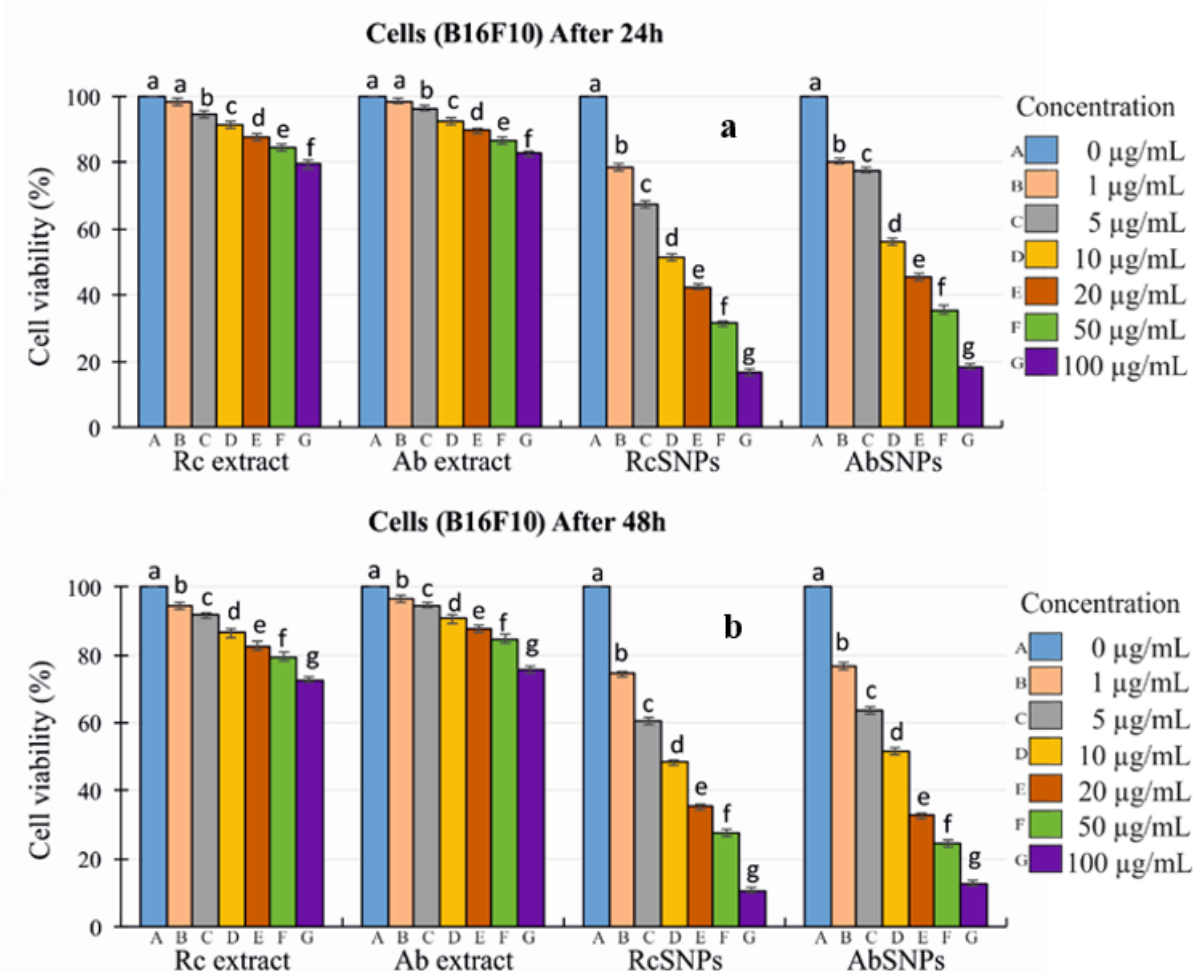

 doi:10.20944/preprints202510.1499.v1

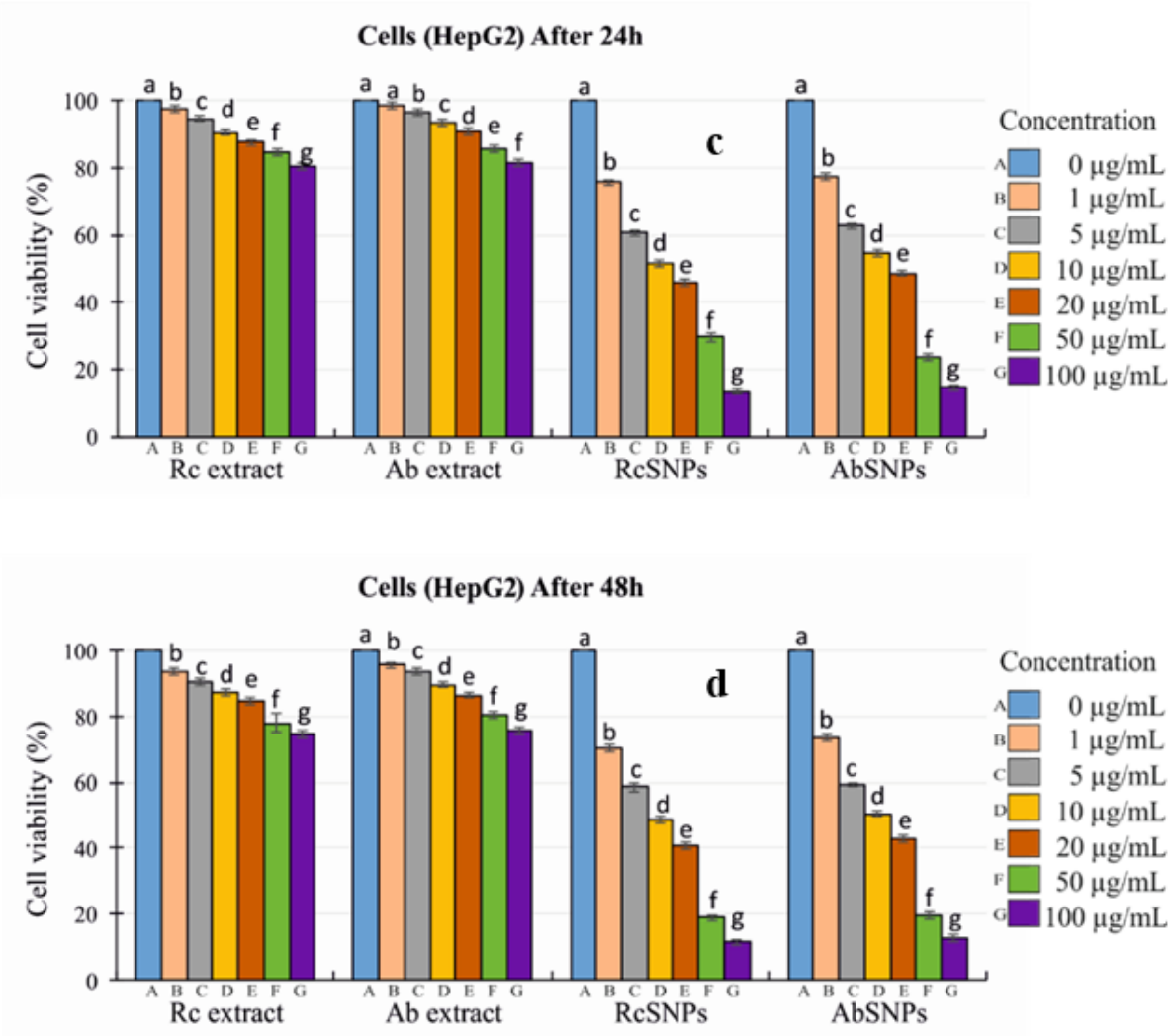

Figure 14. Cytotoxic activity of *Ricinus communis* (Rc) and *Aloe barbadensis* (Ab) extracts and their corresponding SNPs against B16F10 and HepG2 cell lines. Panels show: (a) Rc and Ab treatments on B16F10 cells after 24 h, (b) B16F10 cells after 48 h, (c) HepG2 cells after 24 h, and (d) HepG2 cells after 48 h. Values with different superscripts (a–j) within the same variable are significantly different ($P < 0.05$).

4. Discussion

4.1. Synthesis and Optimization of Silver Nanoparticles (SNPs)

Ricinus communis and *Aloe barbadensis* plant extracts contain a variety of bioactive compounds, including alkaloids, glycosides, flavonoids, tannins, saponins, terpenoids, phenols, and reducing sugars, which can effectively reduce silver ions to silver nanoparticles (SNPs) and act as natural capping agents [54–56]. These phytochemicals highlight the medicinal potential of *R. communis* and *A. barbadensis*, as supported by previous studies [57,58]. In particular, the phenolic compounds exhibit redox properties that contribute to their antioxidant activity [59,60] and are largely responsible for the biological effects of the extracts. Consequently, both extracts are expected to demonstrate significant antioxidant, anti-inflammatory, and antibacterial activities. Literature indicates that phenolic and flavonoid compounds are more efficiently extracted in aqueous solutions and are biosynthesized via the phenylpropanoid pathway from phenylalanine [61]. The current findings align with total phenolic content (TPC) results reported for plant extracts from *Calophyllum tomentosum*, bearberry, olive leaves, *Euodia malayana*, *Gnetum gnemon*, *Haloxylon scoparium*, and *Khaya senegalensis* [7,62–66].

 doi:10.20944/preprints202510.1499.v1

The color change of the reaction mixture serves as the initial indication of silver nanoparticle (SNP) formation. In this study, the solution color changed from yellowish to light brown and ultimately to dark brown (Figure 2.1), consistent with previous reports [67,68]. This color development is attributed to surface plasmon resonance (SPR), which arises from the collective oscillation of conduction electrons induced by an electromagnetic field interacting with electrons at the surface of metallic nanoparticles [69]. The SPR band's position and width depend on the nanoparticle's size, shape, the metal's dielectric properties, and the surrounding environment [70]. UV–visible (UV–vis) spectroscopy, a simple and widely used technique, confirmed SNP synthesis, with SPR bands observed near 435 nm for *R. communis* and 442 nm for *A. barbadensis*, in agreement with the literature [71,72]. At higher silver nitrate concentrations, larger SNPs were formed, accompanied by broader SPR bands, likely due to the inhibitory effect of excess silver ions on nanoparticle formation, which slowed the reaction rate.

Another study reported that increasing the silver nitrate concentration enhanced silver nanoparticle (AgNP) synthesis, as evidenced by the intensified color of the reaction mixture due to the aggregation of silver ions, leading to greater nanoparticle formation [73]. Using 1 mM silver nitrate with *Solanum trilobatum* extract produced monodisperse AgNPs without aggregation. However, at 2–4 mM silver nitrate, a spectral band appeared at 460 nm, and at 5 mM, the SPR band shifted to 500 nm, indicating polydispersity and larger particle sizes. Increasing silver nitrate concentration generally broadens the plasmon resonance band [74]. Similarly, increasing the leaf extract concentration to 4 mL (Figure 2b, g) resulted in a red shift of the SPR band and subtle changes in absorbance, reflecting changes in particle size [64]. Higher extract concentrations also increased absorption intensity. UV–vis spectroscopy is thus widely accepted for monitoring nanoparticles of controlled size and shape in aqueous suspensions. These observations are consistent with previous reports, where AgNP synthesis using *Pithophora dogonia* and *Cochlospermum religiosum* extracts exhibited SPR bands around 445 nm [75,76]. Collectively, these findings suggest that *R. communis* and *A. barbadensis* leaf extracts enable rapid and efficient synthesis of AgNPs, as confirmed by their UV–vis absorption spectra.

Similar observations were reported for silver nanoparticles (AgNPs) synthesized using *Malus domestica* [77], *Parthenium hysterophorus* [78], *Abies alba* and *Pinus sylvestris* [79]. Increasing the concentration of plant extract enhanced the absorption peak, indicating a greater reduction of silver ions and the formation of stable, well-defined AgNPs. At higher extract concentrations, phytochemicals not only act as reducing agents but also coat the nanoparticles, preventing agglomeration and improving stability [80].

The synthesis of silver nanoparticles (SNPs) was found to increase with reaction time; however, prolonged reaction periods can lead to instability due to agglomeration and increased particle size. Logeswari et al. reported SNP formation at 24–48 h at 37 °C using 1 mM silver nitrate and ammonium solution with ethanolic extracts of *Centella asiatica*, *Syzygium cumini*, *Citrus sinensis*, and *Solanum trilobatum*. The reaction mixture color changed from yellow to dark brown, and the resulting SNPs were irregular in shape with sizes ranging from 41–53 nm [71]. In contrast, SNPs synthesized from *Ocimum sanctum* began forming within 3 min, reaching optimal levels at 30 min. Absorption spectra recorded at 60, 90, and 120 min showed no significant differences, although the absorption peak bandwidth increased with nanoparticle polydispersity [81].

pH also plays a critical role in SNP synthesis. Lower pH values favor the formation of larger particles due to aggregation, whereas higher pH values promote nucleation and produce smaller, well-dispersed SNPs. For example, *Garcinia mangostana* extract produced large aggregates at pH 4, while highly dispersed small SNPs were obtained at pH 8. Neutral pH was found to be optimal for SNP formation [67]. Supporting this, Iravani Zolfaghari investigated SNP synthesis using pine bark extract with varying silver nitrate concentrations and phosphate buffers across a pH range of 3–11, confirming the significant influence of pH on nanoparticle size and dispersion [82].

The effect of pH on SNP synthesis has been widely reported. Using *Acalypha indica* extract, no SNP formation was observed under acidic conditions, whereas rapid color change and SNP

 doi:10.20944/preprints202510.1499.v1

formation occurred under alkaline conditions, with an absorption peak shifting to 500 nm; however, at pH 13, immediate aggregation was observed. At neutral pH, the reaction commenced upon addition of silver nitrate, with SNP formation completed within 30 min of incubation [83]. Similarly, when *Crataegus douglasii* fruit extract was used, the absorption wavelength decreased from pH 2–6 over 24 h. No SNPs were formed at pH 2 due to aggregation, while alkaline conditions significantly reduced aggregation [84]. For *Solanum trilobatum* extract, pH 5.8 inhibited nanoparticle synthesis due to limited accessibility of functional groups. At pH 8.8, a broad absorption band appeared at 480 nm, whereas at pH 7.8, a narrow peak at 440 nm corresponded to maximum SNP production [85].

Ndikau et al. synthesized spherical and stable silver nanoparticles (SNPs) using 0.001 M *Citrullus lanatus* extract and 250 g/L silver nitrate at 80 °C and pH 10 in a 4:5 ratio, obtaining nanoparticles with a diameter of 17.96 ± 0.16 nm [86]. Kumar et al. reported SNP synthesis at room temperature using 10% *Annona squamosa* extract and 1 mM silver nitrate for 4 h, producing spherical to irregular-shaped nanoparticles with an average size of 35 ± 5 nm [87]. Similarly, Das et al. prepared SNPs from *Sesbania grandiflora* leaves with 1 mM silver nitrate by incubating in the dark at 37 °C; the resulting spherical nanoparticles (10–25 nm) remained stable at room temperature for six months [88].

The effect of temperature on SNP synthesis has been extensively studied. Using *Solanum trilobatum*, no SPR band was observed at 20 °C, whereas distinct SPR peaks appeared at 35, 45, and 70 °C, with the highest yield achieved at the highest temperature. The SPR peak shifted from 460 nm to 440 nm (blue shift), indicating that higher temperatures strongly influence nanoparticle properties [89]. Generally, increasing the temperature (25–150 °C) enhances SNP production, intensifies absorbance, and reduces nanoparticle size, resulting in a more pronounced SPR band [45]. Similarly, SNP synthesis from *Garcinia mangostana* leaf extract between 37–90 °C showed increased nanoparticle yield with rising temperature. Initially, particle size decreased due to reduced aggregation, but above 75 °C, crystal formation around the nuclei caused a decline in absorbance [90].

In the present study, the optimized conditions for *R. communis* silver nanoparticles (RcSNPs) synthesis were 1 mM $AgNO_3$, 2 mL leaf extract, 25 °C, pH 11, and a 5 min reaction time. For *A. barbadensis* silver nanoparticles (AbSNPs), the optimal conditions were 2 mM $AgNO_3$, 1 mL leaf extract, 25 °C, pH 12, and a 3 min reaction time.

4.2. Proposed Mechanism for RcSNPs and AbSNPs Synthesis

In this study, *R. communis* and *A. barbadensis* aqueous leaf extracts were used for the plant-mediated synthesis of silver nanoparticles (SNPs). The process is initiated by the phenolic compounds and flavonoids present in the extracts. Phytochemical analysis of *R. communis* extract revealed the presence of alkaloids, phenolic compounds, flavonoids, sugars, and proteins. Among these, phenolic compounds and flavonoids act as efficient reducing agents, whereas proteins and certain other phytochemicals serve as capping and stabilizing agents for SNPs [91]. The enol groups of phenolic compounds and flavonoids can release electrons through O–H bond cleavage, and these electrons reduce Ag^+ to Ag^0. Additionally, proteins in *R. communis* extract are expected to stabilize the nanoparticles by capping them [92]. FTIR analysis supports this mechanism, indicating the involvement of hydroxyl and amide groups in the reduction and capping of RcSNPs.

Previous studies indicate that metallic ion reduction can occur via oxidation of amino or hydroxyl groups [93], or through specific terpenoids and alkaloids present in *A. barbadensis* extract. In this case, hydroxyl groups in alkaloids, glycosides, and steroids transfer electrons to silver ions, facilitating SNP formation [94]. Reduction of metallic ions is often achieved through oxidation of O–H groups to carbonyl groups [95]. The resulting nanoparticles may bind to proteins released from the *A. barbadensis* extract, producing protein-capped SNPs. The proposed reaction can be depicted as:

$$AgNO_3 \Rightarrow Ag^+ + NO_3^-$$
$$Ag^+ + e^- \Rightarrow Ag \qquad (2)$$

Stability studies confirmed that SNPs synthesized using these plant extracts are more stable than those produced via conventional chemical methods. These findings are consistent with reports from

 doi:10.20944/preprints202510.1499.v1

other researchers, highlighting the effectiveness of plant-mediated synthesis in producing stable, protein-capped nanoparticles.

4.3. Characterization of SNPs

Dynamic light scattering (DLS) was employed to determine the particle size distribution of the synthesized nanoparticles, providing information on the hydrodynamic diameter, size distribution, and polydispersity index (PDI). The measured negative zeta potential values indicate that the nanoparticles are highly stable, and dispersity analysis confirmed that they are well distributed. These findings are consistent with previously reported values [96] and correlate with UV–vis spectroscopy results. According to Gengan et al., a zeta potential greater than +30 mV or less than –30 mV reflects high colloidal stability [97]. Negative values typically arise from the incorporation of bioactive molecules from the plant extract [98], which induce strong electrostatic repulsion between nanoparticles and prevent aggregation [99]. The observed strong negative zeta potential may result from the shielding effect of biologically active plant compounds [100].

Biogenic SNPs are further stabilized through capping by phenolic compounds present in the leaf extracts, which also facilitate the reduction of Ag^{+} ions. To identify the phenolic constituents involved in capping, FTIR analysis was performed on RcSNPs, AbSNPs, and their respective leaf extracts. The analysis confirmed the presence of plant-derived phenolic functional groups on the nanoparticle surface, contributing to the excellent stability profile of the prepared SNPs [101,102].

The morphology and size distribution of silver nanoparticles (SNPs) are critical determinants of their physicochemical properties and biological activities [103]. In this study, SEM revealed that the synthesized SNPs exhibited diverse morphologies, including spherical, cubic, triangular, and rectangular forms. While the particles were relatively well distributed, some agglomeration was observed, likely due to limited stabilization from weak capping agents. TEM analysis further confirmed that the majority of nanoparticles were spherical, consistent with UV–vis and SEM observations, and indicated smaller particle sizes (15–20 nm for RcSNPs and 23–28 nm for AbSNPs).

Recent studies have emphasized the importance of nanoparticle size and shape in biological applications. Nanoparticles within the 1–100 nm range, such as those obtained here, provide a high surface area to volume ratio, which enhances interactions with microbial cells and biological targets [104]. Spherical nanoparticles, in particular, exhibit lower surface energy and higher thermodynamic stability, contributing to uniform dispersion and consistent bioactivity [105]. The presence of triangular and cubic morphologies may further enhance antimicrobial and antioxidant activities due to higher surface energy and increased reactive sites [106].

Agglomeration, as observed in some particles, is a common challenge in green nanoparticle synthesis. It can reduce the effective surface area and potentially decrease biological efficacy [107]. Factors influencing agglomeration include the concentration and type of capping agents, pH, and ionic strength of the synthesis medium. Optimizing these parameters can enhance particle stability and maintain the desirable nanoscale features for biomedical applications [108].

Overall, the SEM and TEM analyses indicate that green synthesis using *Ricinus communis* and *Aloe barbadensis* leaf extracts produces predominantly spherical, uniformly sized SNPs with minor agglomeration. The diversity in shapes and nanoscale dimensions suggests a potential for enhanced biological activity, supporting their use in antimicrobial, antioxidant, anti-inflammatory, and anticancer applications [109]. Future work may focus on fine-tuning synthesis conditions to minimize agglomeration and improve nanoparticle stability.

Thermogravimetric analysis (TGA) and differential scanning calorimetry (DSC) were employed to assess the thermal stability and compositional characteristics of the silver nanoparticles (SNPs) synthesized using *R. communis* and *A. barbadensis* leaf extracts. TGA revealed an initial weight loss around 90 °C, indicative of the desorption of surface-bound biological compounds, such as proteins and polyphenols, which play a crucial role in the reduction and stabilization of silver ions during nanoparticle synthesis [110]. The DSC analysis demonstrated a single-stage endothermic peak corresponding to the decomposition of these organic stabilizers, aligning with the TGA results. This

 doi:10.20944/preprints202510.1499.v1

congruence suggests that the phytochemicals not only reduce Ag^{+} to Ag^{0} but also contribute to the thermal stability of the nanoparticles by forming a protective layer around them [111,112].

Collectively, the TGA and DSC analyses indicate that the synthesized SNPs possess good thermal stability up to approximately 90 °C, which is advantageous for their potential applications in various biomedical and industrial fields [113]. The presence of plant-derived stabilizing agents further underscores the eco-friendly nature of the green synthesis method employed.

4.4. Therapeutic Evaluation of SNPs

The antimicrobial activity of SNPs was evaluated against various pathogenic strains. The diameter of inhibition zones increased with higher SNP concentrations, indicating a dose-dependent effect [114]. Smaller nanoparticles, with their larger surface area, exhibited enhanced bactericidal activity [115]. The proposed mechanisms underlying the antimicrobial properties of plant-synthesized SNPs include: (i) interaction of silver ions with thiol-containing proteins, leading to protein denaturation and loss of function; (ii) binding to negatively charged DNA, causing structural damage and inhibiting replication; (iii) inhibition of respiratory enzymes (e.g., hydrogenase II) and cofactors (e.g., NADH), disrupting cellular respiration; (iv) induction of reactive oxygen species (ROS) such as hydroxyl radicals and superoxide anions, interfering with the cell respiration cycle; and (v) direct penetration of silver ions into microbial cell walls, resulting in cell death [116–118]. Optimized RcSNPs and AbSNPs exhibited superior antimicrobial activity compared with previously reported *R. communis* and *A. barbadensis*-derived nanoparticles, attributed to their smaller size, improved stability, and spherical morphology [119–123].

In addition to antimicrobial effects, SNPs demonstrated antiplatelet activity. Drugs such as aspirin and heparin, commonly used to prevent blood clotting in conditions like atherosclerosis and myocardial infarction, are associated with severe bleeding complications [124]. SNPs can modulate platelet activity, inhibiting activation and aggregation, offering a potential alternative approach to controlled antithrombotic therapy [125–128].

The anti-inflammatory activity of SNPs was evaluated using the protein denaturation assay. Leaf extract–encapsulated SNPs significantly inhibited bovine serum albumin (BSA) denaturation, even at lower concentrations than standard anti-inflammatory agents. This effect is likely due to the synergistic action of SNPs and phytochemicals in *R. communis* and *A. barbadensis*, which also exhibited substantial antiprotease activity [129–132]. Protein denaturation is a well-established cause of inflammation, as it results in loss of biological activity and, in some arthritic conditions, the production of autoantigens. Denaturation involves alterations in hydrogen bonding, disulfide linkages, electrostatic interactions, and hydrophobicity [133].

The antioxidant potential of SNPs was evaluated using DPPH and H_2O_2 scavenging assays. Free radicals contribute to numerous human diseases, including arthritis, atherosclerosis, reperfusion injury, and cancer [134,135]. At higher concentrations, SNPs effectively scavenged DPPH radicals by electron donation, while also demonstrating greater reducing power than ascorbic acid. In the presence of H_2O_2, SNPs promoted ROS generation, including hydroxyl radicals, which could induce oxidative stress through mitochondrial pathways, cathepsin leakage, and potassium efflux [136–139]. These results align with prior reports on H_2O_2 scavenging by *Abutilon indicum* leaf extract [140].

SNPs also exhibited notable anti-tyrosinase activity. Tyrosinase, a copper-containing metalloenzyme, catalyzes the oxidation of tyrosine to dihydroxyphenylalanine (DOPA) and subsequently to DOPA quinone, which are key intermediates in melanin biosynthesis [141,142]. Overactivity of tyrosinase can lead to hyperpigmentation disorders, including melasma, freckles, and age spots. Biogenic RcSNPs and AbSNPs demonstrated significant inhibition of tyrosinase activity, which is likely attributed to the functional groups from plant phytochemicals capping the nanoparticle surfaces [143]. These capping molecules may interact with the copper active site of tyrosinase or with the substrate binding site, thereby preventing enzymatic oxidation of tyrosine. This dual mechanism—physical adsorption of the enzyme onto the nanoparticle surface and chemical

 doi:10.20944/preprints202510.1499.v1

interaction via bioactive functional groups-enhances the potential of these SNPs as natural skin-lightening or depigmenting agents in cosmetic and therapeutic applications [144].

The cytotoxicity and anticancer potential of RcSNPs and AbSNPs were assessed using the MTT assay, which demonstrated a significant reduction in cell viability in a dose-dependent manner. The SNPs induced apoptosis via mitochondrial membrane disruption and ROS production, activating the caspase-9/3 signaling pathway [145–147]. The release of cytochrome c from the mitochondrial intermembrane space further contributed to mitochondrial stress, while apoptosis-regulating genes Bcl-2 and Bax mediated the loss of mitochondrial integrity [148].

Compared with previously reported in vitro studies on *R. communis* and *A. barbadensis*, the cytotoxic effects observed in this study were more pronounced, indicating that these biogenic SNPs are promising candidates for anticancer applications [56,119,123,129,149,150]. The incorporation of phytochemicals during green synthesis likely enhances the nanoparticles' stability and bioactivity, contributing to their improved therapeutic profile.

Collectively, these findings demonstrate that biogenic RcSNPs and AbSNPs possess potent antimicrobial, antiplatelet, anti-inflammatory, antioxidant, anti-tyrosinase, and anticancer activities, underpinned by the synergistic effects of phytochemical capping and nanoscale properties.

5. Conclusions

This study demonstrates the efficient green synthesis of silver nanoparticles using *Ricinus communis* and *Aloe barbadensis* leaf extracts as reducing and capping agents. Optimized conditions yielded uniformly sized, spherical nanoparticles with enhanced stability. RcSNPs and AbSNPs exhibited potent antibacterial, antifungal, anti-inflammatory, antioxidant, anticoagulant, anti-tyrosinase, and cytotoxic activities, surpassing the efficacy of plant extracts and comparable reports. These findings position phytogenic SNPs as promising candidates for multifunctional biomedical and biopharmaceutical applications, offering broad therapeutic efficacy with reduced toxicity. Future work should validate their in vivo performance and explore integration into advanced drug delivery systems.

Author Contributions: Conceptualization, A.A., and W.T, G.F.G.; methodology, A.A.; formal analysis and investigation, A.A.; resources, W.T., G.F.G; data curation, A.A.; writing—original draft preparation, A.A.; writing—review and editing, A.A., and W.T.; visualization, A.A.; supervision, W.T., G.F.G; project administration, W.T., G.F.G.,; funding acquisition, W.T. All authors have read and agreed to the published version of the manuscript.

Funding: This work received no external funding.

Data Availability Statement: The datasets generated during and/or analysed during the current study are available from the corresponding author on reasonable request.

Acknowledgments: A.A. is grateful for scholarships and funding from the Shanxi Agricultural University, China and Professor Wen-xia tian to support this research work.

Conflicts of Interest: The authors declare no conflicts of interest.

References

1. Hamida, R.S.; Abdelmeguid, N.E.; Ali, M.A.; Bin-Meferij, M.M.; Khalil, M.I. Synthesis of silver nanoparticles using a novel cyanobacteria Desertifilum sp. extract: their antibacterial and cytotoxicity effects. *Int. J. Nanomed*. **2020**, 49-63.
2. Sriramulu, M.; Sumathi, S. Photocatalytic, antioxidant, antibacterial and anti-inflammatory activity of silver nanoparticles synthesised using forest and edible mushroom. *Adv. Nat. Sci. Nanosci. Nanotechnol.* **2017**, *8*, 045012.

 doi:10.20944/preprints202510.1499.v1

3. Lateef, A.;S Folarin, B.I.; Oladejo, S.M.; Akinola, P.O.; Beukes, L.S.; Gueguim-Kana, E.B. Characterization, antimicrobial, antioxidant, and anticoagulant activities of silver nanoparticles synthesized from Petiveria alliacea L. leaf extract. *Prep. Biochem. Biotechnol.* **2018**, *48*, 646-652.
4. Odeniyi, M.A.; Okumah, V.C.; Adebayo-Tayo, B.C.; Odeniyi, O.A. Green synthesis and cream formulations of silver nanoparticles of Nauclea latifolia (African peach) fruit extracts and evaluation of antimicrobial and antioxidant activities. *Sustain. Chem. Pharm.* **2020**, *15*, 100197.
5. Fatima, R.; Priya, M.; Indurthi, L.; Radhakrishnan, V.; Sudhakaran, R. Biosynthesis of silver nanoparticles using red algae Portieria hornemannii and its antibacterial activity against fish pathogens. *Microb. Pathog.* **2020**, *138*, 103780.
6. Wypij, M.; Czarnecka, J.; Świecimska, M.; Dahm, H.; Rai, M.; Golinska, P. Synthesis, characterization and evaluation of antimicrobial and cytotoxic activities of biogenic silver nanoparticles synthesized from Streptomyces xinghaiensis OF1 strain. *World J. Microbiol. Biotechnol.* **2018**, *34*, 23.
7. Govindappa, M.; Hemashekhar, B.; Arthikala, M.-K.; Rai, V.R.; Ramachandra, Y. Characterization, antibacterial, antioxidant, antidiabetic, anti-inflammatory and antityrosinase activity of green synthesized silver nanoparticles using Calophyllum tomentosum leaves extract. *Results Phys.* **2018**, *9*, 400-408.
8. Siddiquee, M.A.; ud din Parray, M.; Mehdi, S.H.; Alzahrani, K.A.; Alshehri, A.A.; Malik, M.A.; Patel, R. Green synthesis of silver nanoparticles from Delonix regia leaf extracts: In-vitro cytotoxicity and interaction studies with bovine serum albumin. *Mater. Chem. Phys.* **2020**, *242*, 122493.
9. Das, P.; Ghosal, K.; Jana, N.K.; Mukherjee, A.; Basak, P. Green synthesis and characterization of silver nanoparticles using belladonna mother tincture and its efficacy as a potential antibacterial and anti-inflammatory agent. *Mater. Chem. Phys.* **2019**, *228*, 310-317.
10. Ravichandran, V.; Vasanthi, S.; Shalini, S.; Shah, S.A.A.; Tripathy, M.; Paliwal, N. Green synthesis, characterization, antibacterial, antioxidant and photocatalytic activity of Parkia speciosa leaves extract mediated silver nanoparticles. *Results Phys.* **2019**, *15*, 102565.
11. Hamedi, S.; Shojaosadati, S.A. Rapid and green synthesis of silver nanoparticles using Diospyros lotus extract: Evaluation of their biological and catalytic activities. *Polyhedron* **2019**, *171*, 172-180.
12. Vanlalveni, C.; Lallianrawna, S.; Biswas, A.; Selvaraj, M.; Changmai, B.; Rokhum, S.L. Green synthesis of silver nanoparticles using plant extracts and their antimicrobial activities: A review of recent literature. *RSC Adv.* **2021**, *11*, 2804-2837.
13. Ahsan, A.; Farooq, M.A. Therapeutic potential of green synthesized silver nanoparticles loaded PVA hydrogel patches for wound healing. *J. Drug Deliv. Sci. Technol.* **2019**, *54*, 101308.
14. Girón-Vázquez, N.; Gómez-Gutiérrez, C.; Soto-Robles, C.; Nava, O.; Lugo-Medina, E.; Castrejón-Sánchez, V.; Vilchis-Nestor, A.; Luque, P. Study of the effect of Persea americana seed in the green synthesis of silver nanoparticles and their antimicrobial properties. *Results Phys*. **2019**, *13*, 102142.
15. Thomas, B.; Vithiya, B.; Prasad, T.; Mohamed, S.; Magdalane, C.M.; Kaviyarasu, K.; Maaza, M. Antioxidant and photocatalytic activity of aqueous leaf extract mediated green synthesis of silver nanoparticles using Passiflora edulis f. flavicarpa. *J. Nanoscience Nanotechnol.* **2019**, *19*, 2640-2648.
16. Kumar, P.V.; Kalyani, R.; Veerla, S.C.; Kollu, P.; Shameem, U.; Pammi, S. Biogenic synthesis of stable silver nanoparticles via Asparagus racemosus root extract and their antibacterial efficacy towards human and fish bacterial pathogens. *Mater. Res. Express* **2019**, *6*, 104008.
17. Singh, P.; Ahn, S.; Kang, J.-P.; Veronika, S.; Huo, Y.; Singh, H.; Chokkaligam, M.; El-Agamy Farh, M.; Aceituno, V.C.; Kim, Y.J. In vitro anti-inflammatory activity of spherical silver nanoparticles and monodisperse hexagonal gold nanoparticles by fruit extract of Prunus serrulata: a green synthetic approach. *Artif. Cells Nanomed. Biotechnol.* **2018**, *46*, 2022-2032.
18. Khosravi, A.; Zarepour, A.; Iravani, S.; Varma, R.S.; Zarrabi, A. Sustainable synthesis: natural processes shaping the nanocircular economy. *Environ. Sci.: Nano* **2024**, *11*, 688-707.
19. Babu, A.T.; Antony, R. Green synthesis of silver doped nano metal oxides of zinc & copper for antibacterial properties, adsorption, catalytic hydrogenation & photodegradation of aromatics. *J. Environ. Chem. Eng*. **2019**, *7*, 102840.
20. Khojasteh, D.; Kazerooni, M.; Salarian, S.; Kamali, R. Droplet impact on superhydrophobic surfaces: A review of recent developments. *J. Ind. Eng. Chem.* **2016**, *42*, 1-14.

 doi:10.20944/preprints202510.1499.v1

21. Kumar, V.; Singh, D.K.; Mohan, S.; Gundampati, R.K.; Hasan, S.H. Photoinduced green synthesis of silver nanoparticles using aqueous extract of Physalis angulata and its antibacterial and antioxidant activity. *J. Environ. Chem. Eng.* **2017**, *5*, 744-756.
22. Sowmyya, T. Spectroscopic investigation on catalytic and bactericidal properties of biogenic silver nanoparticles synthesized using Soymida febrifuga aqueous stem bark extract. *J. Environ. Chem. Eng.* **2018**, *6*, 3590-3601.
23. Vickers, N.J. Animal communication: when i'm calling you, will you answer too? *Curr. Biol.* **2017**, *27*, R713-R715.
24. Parlinska-Wojtan, M.; Kus-Liskiewicz, M.; Depciuch, J.; Sadik, O. Green synthesis and antibacterial effects of aqueous colloidal solutions of silver nanoparticles using camomile terpenoids as a combined reducing and capping agent. *Bioprocess Biosyst. Eng.* **2016**, *39*, 1213-1223.
25. Melo, P.S.; Massarioli, A.P.; Denny, C.; dos Santos, L.F.; Franchin, M.; Pereira, G.E.; de Souza Vieira, T.M.F.; Rosalen, P.L.; de Alencar, S.M. Winery by-products: Extraction optimization, phenolic composition and cytotoxic evaluation to act as a new source of scavenging of reactive oxygen species. *Food Chem.* **2015**, *181*, 160-169.
26. Raota, C.S.; Cerbaro, A.F.; Salvador, M.; Delamare, A.P.L.; Echeverrigaray, S.; da Silva Crespo, J.; da Silva, T.B.; Giovanela, M. Green synthesis of silver nanoparticles using an extract of Ives cultivar (Vitis labrusca) pomace: Characterization and application in wastewater disinfection. *J. Environ. Chem. Eng.* **2019**, *7*, 103383.
27. Behravan, M.; Panahi, A.H.; Naghizadeh, A.; Ziaee, M.; Mahdavi, R.; Mirzapour, A. Facile green synthesis of silver nanoparticles using Berberis vulgaris leaf and root aqueous extract and its antibacterial activity. *Int. J. Biol. Macromol.* **2019**, *124*, 148-154.
28. Azad, A.; Zafar, H.; Raza, F.; Sulaiman, M. Factors influencing the green synthesis of metallic nanoparticles using plant extracts: a comprehensive review. *Pharm. Fronts* **2023**, *5*, e117-e131.
29. Bhatnagar, S.; Aoyagi, H. Current overview of the mechanistic pathways and influence of physicochemical parameters on the microbial synthesis and applications of metallic nanoparticles. *Bioprocess Biosyst. Eng.* **2025**, 1-22.
30. Evans, W.C. Trease and Evans' pharmacognosy. *Gen. Pharmacol.* **1997**, *2*, 291.
31. Urquiaga, I.; Leighton, F. Plant polyphenol antioxidants and oxidative stress. *Biol. Res.* **2000**, *33*, 55-64.
32. Obadoni, B.; Ochuko, P. Phytochemical studies and comparative efficacy of the crude extracts of some haemostatic plants in Edo and Delta States of Nigeria. *Glob. J. Pure Appl. Sci.* **2002**, *8*, 203-208.
33. Al-Dhabi, N.A.; Ponmurugan, K.; Jeganathan, P.M. Development and validation of ultrasound-assisted solid-liquid extraction of phenolic compounds from waste spent coffee grounds. *Ultrason. Sonochem.* **2017**, *34*, 206-213.
34. Ojo, O.A.; Oyinloye, B.E.; Ojo, A.B.; Afolabi, O.B.; Peters, O.A.; Olaiya, O.; Fadaka, A.; Jonathan, J.; Osunlana, O. Green synthesis of silver nanoparticles (AgNPs) using Talinum triangulare (Jacq.) Willd. leaf extract and monitoring their antimicrobial activity. *J. Bionanosci.* **2017**, *11*, 292-296.
35. Kumar, B.; Smita, K.; Cumbal, L.; Debut, A. Green synthesis of silver nanoparticles using Andean blackberry fruit extract. *Saudi J. Biol. Sci.* **2017**, *24*, 45-50.
36. Yildirim, K.; Atas, C.; Simsek, E.; Coban, A.Y. The effect of inoculum size on antimicrobial susceptibility testing of Mycobacterium tuberculosis. *Microbiol. Spectr.* **2023**, *11*, e00319-00323.
37. BEHERA, M.; SOREN, S.; SINGH, N.R.; SIPRA, B.; SETHI, G.; MAHANANDIA, S.; PRADHAN, B.; BHANJADEO, M. Green Synthesis of Bovine Serum Albumin Conjugated Silver Nanoparticles at Different Temperatures and Evaluation of Their Antioxidant Activity. *Indian J. Pharm. Sci.* **2024**, *86*.
38. Banik, S.; Biswas, S.; Karmakar, S. Extraction, purification, and activity of protease from the leaves of Moringa oleifera. *F1000Res.* **2018**, *7*, 1151.
39. Prem, P.; Naveenkumar, S.; Kamaraj, C.; Ragavendran, C.; Priyadharsan, A.; Manimaran, K.; Alharbi, N.S.; Rarokar, N.; Cherian, T.; Sugumar, V. Valeriana jatamansi root extract a potent source for biosynthesis of silver nanoparticles and their biomedical applications, and photocatalytic decomposition. Green Chem. Lett. Rev. **2024**, *17*, 2305142.

 doi:10.20944/preprints202510.1499.v1

40. Shankar, S.; Murthy, A.N.; Rachitha, P.; Raghavendra, V.B.; Sunayana, N.; Chinnathambi, A.; Alharbi, S.A.; Basavegowda, N.; Brindhadevi, K.; Pugazhendhi, A. RETRACTED: Silk sericin conjugated magnesium oxide nanoparticles for its antioxidant, anti-aging, and anti-biofilm activities. **2023**.
41. Pathak, P.; Shukla, P.; Kanshana, J.S.; Jagavelu, K.; Sangwan, N.S.; Dwivedi, A.K.; Dikshit, M. Standardized root extract of Withania somnifera and Withanolide A exert moderate vasorelaxant effect in the rat aortic rings by enhancing nitric oxide generation. *J. Ethnopharmacol.* **2021**, *278*, 114296.
42. Alemu, B.; Molla, M.D.; Tezera, H.; Dekebo, A.; Asmamaw, T. Phytochemical composition and in vitro antioxidant and antimicrobial activities of Bersama abyssinica F. seed extracts. *Sci. Rep.* **2024**, *14*, 6345.
43. Chandrasekhar, N.; Vinay, S. Yellow colored blooms of Argemone mexicana and Turnera ulmifolia mediated synthesis of silver nanoparticles and study of their antibacterial and antioxidant activity. *Appl. Nanosci.* **2017**, *7*, 851-861.
44. Giridasappa, A.; Ismail, S.M.; Gopinath, S. Antioxidant, Bactericidal, Antihemolytic, and Anticancer Assessment Activities of Al2O3, SnO2, and Green Synthesized Ag and CuO NPs. In *Handbook of Sustainable Materials: Modelling, Characterization, and Optimization*; CRC Press: 2023; pp. 367-398.
45. Shahzadi, S.; Fatima, S.; Shafiq, Z.; Janjua, M.R.S.A. A review on green synthesis of silver nanoparticles (SNPs) using plant extracts: a multifaceted approach in photocatalysis, environmental remediation, and biomedicine. *RSC Adv.* **2025**, *15*, 3858-3903.
46. Mughal, S.S. Role of silver nanoparticles in colorimetric detection of biomolecules. *Authorea Preprints* **2022**.
47. Alim-Al-Razy, M.; Bayazid, G.A.; Rahman, R.U.; Bosu, R.; Shamma, S.S. Silver nanoparticle synthesis, UV-Vis spectroscopy to find particle size and measure resistance of colloidal solution. In Proceedings of the Journal of Physics: Conference Series, 2020; p. 012020.
48. Gao, C.; Lu, Z.; Liu, Y.; Zhang, Q.; Chi, M.; Cheng, Q.; Yin, Y. Highly stable silver nanoplates for surface plasmon resonance biosensing. *Angew. Chem. Int. Ed.* **2012**, *51*, 5629-5633.
49. Jia, Z.; Li, J.; Gao, L.; Yang, D.; Kanaev, A. Dynamic light scattering: a powerful tool for in situ nanoparticle sizing. *Colloids Interfaces* **2023**, *7*, 15.
50. Sun, Q.; Cai, X.; Li, J.; Zheng, M.; Chen, Z.; Yu, C.-P. Green synthesis of silver nanoparticles using tea leaf extract and evaluation of their stability and antibacterial activity. *Colloids Surf. A: Physicochem. Eng. Asp.* **2014**, *444*, 226-231.
51. Kumaran, N.S. In vitro anti-inflammatory activity of silver nanoparticle synthesized Avicennia marina (Forssk.) Vierh.: A green synthetic approach. *Int. J. Green Pharm.* **2018**, *12*.
52. Yakop, F.; Abd Ghafar, S.A.; Yong, Y.K.; Saiful Yazan, L.; Mohamad Hanafiah, R.; Lim, V.; Eshak, Z. Silver nanoparticles Clinacanthus Nutans leaves extract induced apoptosis towards oral squamous cell carcinoma cell lines. Artif. Cells Nanomed. Biotechnol. **2018**, *46*, 131-139.
53. Nasrollahzadeh, M.; Issaabadi, Z.; Sajadi, S.M. Green synthesis of the Ag/Al2O3 nanoparticles using Bryonia alba leaf extract and their catalytic application for the degradation of organic pollutants. J. Mater. Sci.: Mater. Electro **2019**, *30*, 3847-3859.
54. Deshpande, B.; Sharma, D.; Pandey, B. Phytochemicals and antibacterial screening of Parthenium hysterophorus. *Indian J. Sci. Res* **2017**, *13*, 199-202.
55. Khan, T.; Ullah, N.; Khan, M.A.; Mashwani, Z.-u.-R.; Nadhman, A. Plant-based gold nanoparticles; a comprehensive review of the decade-long research on synthesis, mechanistic aspects and diverse applications. *Adv. Colloid Interface Sci.* **2019**, *272*, 102017.
56. Abomughaid, M.M.; Teibo, J.O.; Akinfe, O.A.; Adewolu, A.M.; Teibo, T.K.A.; Afifi, M.; Al-Farga, A.M.H.; Al-kuraishy, H.M.; Al-Gareeb, A.I.; Alexiou, A. A phytochemical and pharmacological review of Ricinus communis L. *Discov. Appl. Sci.* **2024**, *6*, 315.
57. Singh, R. Chemotaxonomy of medicinal plants: possibilities and limitations. In *Natural products and drug discovery*; Elsevier: 2018; pp. 119-136.
58. Dharajiya, D.; Pagi, N.; Jasani, H.; Patel, P. Antimicrobial activity and phytochemical screening of Aloe vera (Aloe barbadensis Miller). *Int J Curr Microbiol App Sci* **2017**, *6*, 2152-2162.
59. Baba, S.A.; Malik, S.A. Determination of total phenolic and flavonoid content, antimicrobial and antioxidant activity of a root extract of Arisaema jacquemontii Blume. *J. Taibah Univ. Sci.* **2015**, *9*, 449-454.

 doi:10.20944/preprints202510.1499.v1

60. Chen, Z.; Świsłocka, R.; Choińska, R.; Marszałek, K.; Dąbrowska, A.; Lewandowski, W.; Lewandowska, H. Exploring the correlation between the molecular structure and biological activities of metal–phenolic compound complexes: research and description of the role of metal ions in improving the antioxidant activities of phenolic compounds. *Int. J. Mol. Sci.* **2024**, *25*, 11775.
61. Dakshayani, S.; Marulasiddeshwara, M.; Sharath Kumar, M.; Raghavendra Kumar, P.; Devaraja, S. Antimicrobial, anticoagulant and antiplatelet activities of green synthesized silver nanoparticles using Selaginella (Sanjeevini) plant extract. *Int. J. Biol. Macromol.* **2019**, *131*, 787-797.
62. Song, X.-C.; Canellas, E.; Asensio, E.; Nerín, C. Predicting the antioxidant capacity and total phenolic content of bearberry leaves by data fusion of UV–Vis spectroscopy and UHPLC/Q-TOF-MS. *Talanta* **2020**, *213*, 120831.
63. Lama-Muñoz, A.; del Mar Contreras, M.; Espínola, F.; Moya, M.; Romero, I.; Castro, E. Content of phenolic compounds and mannitol in olive leaves extracts from six Spanish cultivars: Extraction with the Soxhlet method and pressurized liquids. *Food Chem* **2020**, *320*, 126626.
64. Ahmed-Gaid, K.; Ahmed-Gaid, N.E.Y.; Hanoun, S.; Chenna, H.; Ghenaiet, K.; Ahmed-Gaid, H.; Hadef, Y. PHENOLIC COMPOUNDS, ANTIOXIDANT, AND ANTIMICROBIAL ACTIVITIES OF METHANOLIC EXTRACT FROM THE SAHARAN ENDEMIC PLANT HALOXYLON SCOPARIUM POMEL. *Bull. Pharm. Sci. Assiut Univ.* **2025**, *48*, 267-276.
65. Marius, L.; Kini, F.; Pierre, D.; Pierre, G.I. In vitro antioxidant activity and phenolic contents of different fractions of ethanolic extract from Khaya senegalensis A. Juss.(Meliaceae) stem barks. *Afr. J. Pharm. Pharmacol.* **2016**, *10*, 501-507.
66. Khawory, M.H.; Amanah, A.; Salin, N.H.; Mohd Subki, M.F.; Mohd Nasim, N.N.; Noordin, M.I.; Wahab, H.A. Effects of Gamma Radiation Treatment on Medicinal Plants for Both Qualitative and Quantitative Analysis of Phenolic Acid. *Available at SSRN 4334860*.
67. Veerasamy, R.; Xin, T.Z.; Gunasagaran, S.; Xiang, T.F.W.; Yang, E.F.C.; Jeyakumar, N.; Dhanaraj, S.A. Biosynthesis of silver nanoparticles using mangosteen leaf extract and evaluation of their antimicrobial activities. *J. Saudi Chem. Soc.* **2011**, *15*, 113-120.
68. Banerjee, P.; Satapathy, M.; Mukhopahayay, A.; Das, P. Leaf extract mediated green synthesis of silver nanoparticles from widely available Indian plants: synthesis, characterization, antimicrobial property and toxicity analysis. *Bioresour. Bioprocess.* **2014**, *1*, 3.
69. Chandran, N.; Bayal, M.; Pilankatta, R.; Nair, S.S. Tuning of surface Plasmon resonance (SPR) in metallic nanoparticles for their applications in SERS. In *Nanomaterials for luminescent devices, sensors, and bio-imaging applications*; Springer: 2021; pp. 39-66.
70. Yadav, M.; Gaur, N.; Wahi, N.; Singh, S.; Kumar, K.; Amoozegar, A.; Sharma, E. Phytochemical-Assisted Fabrication of Biogenic Silver Nanoparticles from Vitex negundo: Structural Features, Antibacterial Activity, and Cytotoxicity Evaluation. *Colloids Interfaces* **2025**, *9*, 55.
71. Kale, G.; Bhatkar, D.; Rokade, S.; Ingle, P.; Patil, R. Green synthesis of silver nanoparticles using Azadirachta indica leaves extract and characterization by UV. *Sustain. Dev.* **2022**, *1695*, 1995-1699.
72. Markus, J.; Wang, D.; Kim, Y.-J.; Ahn, S.; Mathiyalagan, R.; Wang, C.; Yang, D.C. Biosynthesis, characterization, and bioactivities evaluation of silver and gold nanoparticles mediated by the roots of Chinese herbal Angelica pubescens Maxim. *Nanoscale Res. Lett.* **2017**, *12*, 46.
73. Kaabipour, S.; Hemmati, S. A review on the green and sustainable synthesis of silver nanoparticles and one-dimensional silver nanostructures. Beilstein J. Nanotechnol. **2021**, *12*, 102-136.
74. Chirumamilla, P.; Dharavath, S.B.; Taduri, S. Eco-friendly green synthesis of silver nanoparticles from leaf extract of Solanum khasianum: optical properties and biological applications. *Appl. Biochem. Biotechnol.* **2023**, *195*, 353-368.
75. Sinha, S.N.; Paul, D.; Halder, N.; Sengupta, D.; Patra, S.K. Green synthesis of silver nanoparticles using fresh water green alga Pithophora oedogonia (Mont.) Wittrock and evaluation of their antibacterial activity. *Appl. Nanosci.* **2015**, *5*, 703-709.
76. Sasikala, A.; Linga Rao, M.; Savithramma, N.; Prasad, T. Synthesis of silver nanoparticles from stem bark of Cochlospermum religiosum (L.) Alston: an important medicinal plant and evaluation of their antimicrobial efficacy. *Appl. Nanosci.* **2015**, *5*, 827-835.

 doi:10.20944/preprints202510.1499.v1

77. Mariadoss, A.V.A.; Ramachandran, V.; Shalini, V.; Agilan, B.; Franklin, J.H.; Sanjay, K.; Alaa, Y.G.; Tawfiq, M.A.-A.; Ernest, D. Green synthesis, characterization and antibacterial activity of silver nanoparticles by Malus domestica and its cytotoxic effect on (MCF-7) cell line. *Microb. Pathog.* **2019**, *135*, 103609.
78. Ahsan, A.; Farooq, M.A.; Ahsan Bajwa, A.; Parveen, A. Green synthesis of silver nanoparticles using Parthenium hysterophorus: optimization, characterization and in vitro therapeutic evaluation. *Molecules* **2020**, *25*, 3324.
79. Macovei, I.; Luca, S.V.; Skalicka-Woźniak, K.; Horhogea, C.E.; Rimbu, C.M.; Sacarescu, L.; Vochita, G.; Gherghel, D.; Ivanescu, B.L.; Panainte, A.D. Silver nanoparticles synthesized from abies alba and pinus sylvestris bark extracts: characterization, antioxidant, cytotoxic, and antibacterial effects. *Antioxidants* **2023**, *12*, 797.
80. Halawani, E.M. Rapid biosynthesis method and characterization of silver nanoparticles using Zizyphus spina christi leaf extract and their antibacterial efficacy in therapeutic application. *J. Biomater. Nanobiotechnol.* **2016**, *8*, 22-35.
81. Logeswari, P.; Silambarasan, S.; Abraham, J. Ecofriendly synthesis of silver nanoparticles from commercially available plant powders and their antibacterial properties. *Sci. Iran.* **2013**, *20*, 1049-1054.
82. Iravani, S.; Zolfaghari, B. Green synthesis of silver nanoparticles using Pinus eldarica bark extract. *Biomed Res. Int.* **2013**, *2013*, 639725.
83. Madaniyah, L.; Fiddaroini, S.; Hayati, E.K.; Rahman, M.F.; Sabarudin, A. Biosynthesis, characterization, and in-vitro anticancer effect of plant-mediated silver nanoparticles using Acalypha indica Linn: In-silico approach. *OpenNano* **2025**, *21*, 100220.
84. Alirezalu, A.; Ahmadi, N.; Salehi, P.; Sonboli, A.; Alirezalu, K.; Mousavi Khaneghah, A.; Barba, F.J.; Munekata, P.E.; Lorenzo, J.M. Physicochemical characterization, antioxidant activity, and phenolic compounds of hawthorn (Crataegus spp.) fruits species for potential use in food applications. *Foods* **2020**, *9*, 436.
85. Arumugam, S.; Ramesh, P. Green synthesis and characterization of zirconium oxide nanoparticles using solanum trilobatum and its photodegradation activity. *Sustain. Chem. Clim. Action* **2025**, *6*, 100086.
86. Ndikau, M.; Noah, N.M.; Andala, D.M.; Masika, E. Green synthesis and characterization of silver nanoparticles using Citrullus lanatus fruit rind extract. *Int. J. Anal. Chem.* **2017**, *2017*, 8108504.
87. Kumar, R.; Roopan, S.M.; Prabhakarn, A.; Khanna, V.G.; Chakroborty, S. Agricultural waste Annona squamosa peel extract: biosynthesis of silver nanoparticles. *Spectrochim. Acta A Mol. Biomol. Spectrosc.* **2012**, *90*, 173-176.
88. Das, J.; Das, M.P.; Velusamy, P. Sesbania grandiflora leaf extract mediated green synthesis of antibacterial silver nanoparticles against selected human pathogens. *Spectrochim. Acta A Mol. Biomol. Spectrosc.* **2013**, *104*, 265-270.
89. Vanaja, M.; Paulkumar, K.; Gnanajobitha, G.; Rajeshkumar, S.; Malarkodi, C.; Annadurai, G. Herbal plant synthesis of antibacterial silver nanoparticles by Solanum trilobatum and its characterization. *Int. J. Met.* **2014**, *2014*, 692461.
90. Sarip, N.A.; Aminudin, N.I.; Danial, W.H. Green synthesis of metal nanoparticles using Garcinia extracts: a review. Environ. Chem. Lett. **2022**, *20*, 469-493.
91. Patel, J.; Kumar, G.S.; Roy, H.; Maddiboyina, B.; Leporatti, S.; Bohara, R.A. From nature to nanomedicine: bioengineered metallic nanoparticles bridge the gap for medical applications. *Discov. Nano* **2024**, *19*, 85.
92. Mintiwab, A.; Jeyaramraja, P. Evaluation of phytochemical components, antioxidant and antibacterial activities of silver nanoparticles synthesized using Ricinus communis leaf extracts. *Vegetos* **2021**, *34*, 606-618.
93. Lim, S.H.; Park, Y. Green synthesis, characterization and catalytic activity of gold nanoparticles prepared using rosmarinic acid. *J. Nanoscience Nanotechnol.* **2018**, *18*, 659-667.
94. Adebayo-Tayo, B.C.; Akinsete, T.O.; Odeniyi, O.A. Phytochemical composition and comparative evaluation of antimicrobial activities of the juice extract of Citrus aurantifolia and its silver nanoparticles. *Niger. J. Pharm. Res.* **2016**, *12*, 59-64.

 doi:10.20944/preprints202510.1499.v1

95. Dawadi, S.; Katuwal, S.; Gupta, A.; Lamichhane, U.; Thapa, R.; Jaisi, S.; Lamichhane, G.; Bhattarai, D.P.; Parajuli, N. Current research on silver nanoparticles: synthesis, characterization, and applications. *J. Nanomater.* **2021**, *2021*, 6687290.
96. Pochapski, D.J.; Carvalho dos Santos, C.; Leite, G.W.; Pulcinelli, S.H.; Santilli, C.V. Zeta potential and colloidal stability predictions for inorganic nanoparticle dispersions: Effects of experimental conditions and electrokinetic models on the interpretation of results. *Langmuir* **2021**, *37*, 13379-13389.
97. Gengan, R.; Anand, K.; Phulukdaree, A.; Chuturgoon, A. A549 lung cell line activity of biosynthesized silver nanoparticles using Albizia adianthifolia leaf. *Colloids Surf. B: Biointerfaces* **2013**, *105*, 87-91.
98. Varadavenkatesan, T.; Selvaraj, R.; Vinayagam, R. Phyto-synthesis of silver nanoparticles from Mussaenda erythrophylla leaf extract and their application in catalytic degradation of methyl orange dye. *J. Mol. Liq.* **2016**, *221*, 1063-1070.
99. Padalia, H.; Moteriya, P.; Chanda, S. Green synthesis of silver nanoparticles from marigold flower and its synergistic antimicrobial potential. *Arab. J. Chem.* **2015**, *8*, 732-741.
100. Salih, A.M.; Al-Qurainy, F.; Khan, S.; Nadeem, M.; Tarroum, M.; Shaikhaldein, H.O. Biogenic silver nanoparticles improve bioactive compounds in medicinal plant Juniperus procera in vitro. *Front. Plant Sci.* **2022**, *13*, 962112.
101. Kumar, D.; Salvi, A.; Thakur, V.; Kharbanda, S.; Sangwan, S.; Thakur, P.; Thakur, A. Aloe vera assisted green synthesis of silver nanoparticles: structural characterization, electrochemical behaviour, and antimicrobial efficiency. *Discov. appl. sci.* **2025**, *7*, 530.
102. Modrzejewska-Sikorska, A.; Konował, E. Silver and gold nanoparticles as chemical probes of the presence of heavy metal ions. *J. Mol. Liq.* **2020**, *302*, 112559.
103. Awaly, S.B.; Osman, N.H.; Farag, H.M.; Yacoub, I.H.; Mahmoud-Aly, M.; Elarabi, N.I.E.; Ahmed, D.S. Evaluation of the morpho-physiological traits and the genetic diversity of durum wheat's salt tolerance induced by silver nanoparticles. *J. agric. environ. int. dev.* **2023**, *117*, 161-184.
104. Dubey, R.K.; Shukla, S.; Hussain, Z. Green synthesis of silver nanoparticles; A sustainable approach with diverse applications. *Zhongguo Ying Yong Sheng Li Xue Za Zhi* **2023**, *39*, e20230007.
105. Anjana, V.; Joseph, M.; Francis, S.; Joseph, A.; Koshy, E.P.; Mathew, B. Microwave assisted green synthesis of silver nanoparticles for optical, catalytic, biological and electrochemical applications. *Artif. Cells Nanomed. Biotechnol.* **2021**, *49*, 438-449.
106. Fahim, M.; Shahzaib, A.; Nishat, N.; Jahan, A.; Bhat, T.A.; Inam, A. Green synthesis of silver nanoparticles: A comprehensive review of methods, influencing factors, and applications. *JCIS Open* **2024**, *16*, 100125.
107. Hussain, I.; Singh, N.; Singh, A.; Singh, H.; Singh, S. Green synthesis of nanoparticles and its potential application. *Biotechnol. Lett.* **2016**, *38*, 545-560.
108. Haridas, E.; Varma, M.; Chandra, G.K. Bioactive silver nanoparticles derived from Carica papaya floral extract and its dual-functioning biomedical application. *Sci. Rep.* **2025**, *15*, 1-14.
109. Aminnezhad, S.; Zonobian, M.A.; Moradi Douki, M.; Mohammadi, M.R.; Azarakhsh, Y. Curcumin and their derivatives with anti-inflammatory, neuroprotective, anticancer, and antimicrobial activities: a review. *Micro Nano Bio Asp.* **2023**, *2*, 25-34.
110. Stanoiu, A.-M.; Bejenaru, C.; Segneanu, A.-E.; Vlase, G.; Bradu, I.A.; Vlase, T.; Mogoşanu, G.D.; Ciocîlteu, M.V.; Biţă, A.; Kostici, R. Design and Evaluation of a Inonotus obliquus–AgNP–Maltodextrin Delivery System: Antioxidant, Antimicrobial, Acetylcholinesterase Inhibitory and Cytotoxic Potential. *Polymers* **2025**, *17*, 2163.
111. Yadav, S.; Kumari, P.; Mahto, S.K. Green synthesis of silver nanoparticles using Momordica dioica leaf extract: characterizing antibacterial, antibiofilm, and catalytic activities. *Transit. Met. Chem.* **2025**, 1-18.
112. Mohanaparameswari, S.; Balachandramohan, M.; Kumar, K.G.; Revathy, M.; Sasikumar, P.; Rajeevgandhi, C.; Vimalan, M.; Pugazhendhi, S.; Batoo, K.M.; Hussain, S. Green synthesis of silver oxide nanoparticles using Plectranthus amboinicus and Solanum trilobatum extracts as an Eco-friendly approach: characterization and antibacterial properties. *J Inorg Organomet Polym* **2024**, *34*, 3191-3211.
113. Leyva-Porras, C.; Cruz-Alcantar, P.; Espinosa-Solís, V.; Martínez-Guerra, E.; Piñón-Balderrama, C.I.; Compean Martínez, I.; Saavedra-Leos, M.Z. Application of differential scanning calorimetry (DSC) and modulated differential scanning calorimetry (MDSC) in food and drug industries. *Polymers* **2019**, *12*, 5.

 doi:10.20944/preprints202510.1499.v1

114. Agnihotri, S.; Mukherji, S.; Mukherji, S. Size-controlled silver nanoparticles synthesized over the range 5–100 nm using the same protocol and their antibacterial efficacy. *Rsc Adv* **2014**, *4*, 3974-3983.
115. Karuna, D.; Dey, P.; Das, S.; Kundu, A.; Bhakta, T. In vitro antioxidant activities of root extract of Asparagus racemosus Linn. *J. Tradit. Complement. Med.* **2018**, *8*, 60-65.
116. Rajeshkumar, S.; Bharath, L. Mechanism of plant-mediated synthesis of silver nanoparticles–a review on biomolecules involved, characterisation and antibacterial activity. *Chem Biol Interact* **2017**, *273*, 219-227.
117. El Badawy, A.M.; Silva, R.G.; Morris, B.; Scheckel, K.G.; Suidan, M.T.; Tolaymat, T.M. Surface charge-dependent toxicity of silver nanoparticles. *Environ. Sci. Technol.* **2011**, *45*, 283-287.
118. Shayo, G.M.; Elimbinzi, E.; Shao, G.N. Preparation methods, applications, toxicity and mechanisms of silver nanoparticles as bactericidal agent and superiority of green synthesis method. *Heliyon* **2024**, *10*.
119. Tippayawat, P.; Phromviyo, N.; Boueroy, P.; Chompoosor, A. Green synthesis of silver nanoparticles in aloe vera plant extract prepared by a hydrothermal method and their synergistic antibacterial activity. *PeerJ* **2016**, *4*, e2589.
120. Vélez, E.; Campillo, G.; Morales, G.; Hincapié, C.; Osorio, J.; Arnache, O. Silver nanoparticles obtained by aqueous or ethanolic aloe Vera extracts: An assessment of the antibacterial activity and mercury removal capability. *J. Nanomater.* **2018**, *2018*, 7215210.
121. Haripriya, S.; Ajitha, P. Antimicrobial efficacy of silver nanoparticles of Aloe vera. **2017**.
122. Urnukhsaikhan, E.; Bold, B.-E.; Gunbileg, A.; Sukhbaatar, N.; Mishig-Ochir, T. Antibacterial activity and characteristics of silver nanoparticles biosynthesized from Carduus crispus. *Sci. Rep.* **2021**, *11*, 21047.
123. Ojha, S.; Sett, A.; Bora, U. Green synthesis of silver nanoparticles by Ricinus communis var. carmencita leaf extract and its antibacterial study. *Adv. Nat. Sci.:Nanosci. Nanotechnol.* **2017**, *8*, 035009.
124. Kitchen, S.; Gray, E.; Mackie, I.; Baglin, T.; Makris, M. Measurement of non-coumarin anticoagulants and their effects on tests of Haemostasis: Guidance from the British Committee for Standards in Haematology. *Br. J. Haematol.* **2014**, *166*.
125. Shrivastava, S.; Bera, T.; Singh, S.K.; Singh, G.; Ramachandrarao, P.; Dash, D. Characterization of antiplatelet properties of silver nanoparticles. *ACS Nano* **2009**, *3*, 1357-1364.
126. Rodrigues, A.S.; Batista, J.G.; Rodrigues, M.Á.; Thipe, V.C.; Minarini, L.A.; Lopes, P.S.; Lugão, A.B. Advances in silver nanoparticles: a comprehensive review on their potential as antimicrobial agents and their mechanisms of action elucidated by proteomics. *Front. Microbiol.* **2024**, *15*, 1440065.
127. Do, H.T.T.; Nguyen, N.P.U.; Saeed, S.I.; Dang, N.T.; Doan, L.; Nguyen, T.T.H. Advances in silver nanoparticles: unraveling biological activities, mechanisms of action, and toxicity. *Appl. Nanosci.* **2025**, *15*, 1.
128. Ibrahim, A.T.A. Toxicological impact of green synthesized silver nanoparticles and protective role of different selenium type on Oreochromis niloticus: hematological and biochemical response. *J. Trace Elem. Med. Biol.* **2020**, *61*, 126507.
129. Nemudzivhadi, V.; Masoko, P. In vitro assessment of cytotoxicity, antioxidant, and anti-inflammatory activities of Ricinus communis (Euphorbiaceae) leaf extracts. *Evid. Based Complement. Alternat. Med.* **2014**, *2014*, 625961.
130. Valderramas, A.C.; Moura, S.H.P.; Couto, M.; Pasetto, S.; Chierice, G.O.; Guimarães, S.A.C.; Zurron, A.C.B.d.P. Antiinflammatory activity of Ricinus communis derived polymer. **2009**.
131. Varghese, R.M.; Kumar, A.; Shanmugam, R. Comparative anti-inflammatory activity of silver and zinc oxide nanoparticles synthesized using Ocimum tenuiflorum and Ocimum gratissimum herbal formulations. *Cureus* **2024**, *16*.
132. Khashan, A.A.; Dawood, Y.; Khalaf, Y.H. Green chemistry and anti-inflammatory activity of silver nanoparticles using an aqueous curcumin extract. *Results Chem.* **2023**, *5*, 100913.
133. Dharmadeva, S.; Galgamuwa, L.S.; Prasadinie, C.; Kumarasinghe, N. In vitro anti-inflammatory activity of Ficus racemosa L. bark using albumin denaturation method. *Ayu* **2018**, *39*, 239-242.
134. Matkowski, A.; Tasarz, P.; Szypuła, E. Antioxidant activity of herb extracts from five medicinal plants from Lamiaceae, subfamily Lamioideae. *J. Med. Plants Res.* **2008**, *2*, 321-330.

 doi:10.20944/preprints202510.1499.v1

135. Silva, F.; Veiga, F.; Cardoso, C.; Dias, F.; Cerqueira, F.; Medeiros, R.; Paiva-Santos, A.C. A rapid and simplified DPPH assay for analysis of antioxidant interactions in binary combinations. *Microchem. J.* **2024**, *202*, 110801.
136. Sohal, J.K.; Saraf, A.; Shukla, K.; Shrivastava, M. Determination of antioxidant potential of biochemically synthesized silver nanoparticles using Aloe vera gel extract. *Plant Sci. Today* **2019**, *6*, 208-217.
137. More, G.K.; Makola, R.T. In-vitro analysis of free radical scavenging activities and suppression of LPS-induced ROS production in macrophage cells by Solanum sisymbriifolium extracts. *Sci. Rep.* **2020**, *10*, 6493.
138. Rana, M.S.; Rayhan, N.M.A.; Emon, M.S.H.; Islam, M.T.; Rathry, K.; Hasan, M.M.; Mansur, M.M.I.; Srijon, B.C.; Islam, M.S.; Ray, A. Antioxidant activity of Schiff base ligands using the DPPH scavenging assay: an updated review. *RSC Adv* **2024**, *14*, 33094-33123.
139. He, W.; Zhou, Y.-T.; Wamer, W.G.; Boudreau, M.D.; Yin, J.-J. Mechanisms of the pH dependent generation of hydroxyl radicals and oxygen induced by Ag nanoparticles. *Biomaterials* **2012**, *33*, 7547-7555.
140. Mata, R.; Nakkala, J.R.; Sadras, S.R. Biogenic silver nanoparticles from Abutilon indicum: their antioxidant, antibacterial and cytotoxic effects in vitro. *Colloids Surf. B Biointerfaces* **2015**, *128*, 276-286.
141. Irfan, A.; Jardan, Y.A.B.; Rubab, L.; Hameed, H.; Zahoor, A.F.; Supuran, C.T. Bacterial tyrosinases and their inhibitors. *Enzymes* **2024**, *56*, 231-260.
142. Mukherjee, P.K.; Biswas, R.; Sharma, A.; Banerjee, S.; Biswas, S.; Katiyar, C. Validation of medicinal herbs for anti-tyrosinase potential. *J Herb Med* **2018**, *14*, 1-16.
143. Özer, Ö.; Mutlu, B.; Kıvçak, B. Antityrosinase activity of some plant extracts and formulations containing ellagic acid. *Pharm Biol* **2007**, *45*, 519-524.
144. Manickam, V.; Mani, G.; Muthuvel, R.; Pushparaj, H.; Jayabalan, J.; Pandit, S.S.; Elumalai, S.; Kaliappan, K.; Tae, J.H. Green fabrication of silver nanoparticles and it's in vitro anti-bacterial, anti-biofilm, free radical scavenging and mushroom tyrosinase efficacy evaluation. Inorg Chem Commun **2024**, *162*, 112199.
145. Verma, S.K.; Jha, E.; Sahoo, B.; Panda, P.K.; Thirumurugan, A.; Parashar, S.; Suar, M. Mechanistic insight into the rapid one-step facile biofabrication of antibacterial silver nanoparticles from bacterial release and their biogenicity and concentration-dependent in vitro cytotoxicity to colon cells. *RSC Adv* **2017**, *7*, 40034-40045.
146. Akter, M.; Sikder, M.T.; Rahman, M.M.; Ullah, A.A.; Hossain, K.F.B.; Banik, S.; Hosokawa, T.; Saito, T.; Kurasaki, M. A systematic review on silver nanoparticles-induced cytotoxicity: Physicochemical properties and perspectives. J Adv Res **2018**, *9*, 1-16.
147. Sati, A.; Mali, S.N.; Ranade, T.N.; Yadav, S.; Pratap, A. Silver Nanoparticles (AgNPs) as a Double-Edged Sword: Synthesis, Factors Affecting, Mechanisms of Toxicity and Anticancer Potentials—An Updated Review till March 2025. *Biol Trace Elem Res* **2025**, 1-52.
148. Garrido, C.; Galluzzi, L.; Brunet, M.; Puig, P.; Didelot, C.; Kroemer, G. Mechanisms of cytochrome c release from mitochondria. *Cell Death Differ* **2006**, *13*, 1423-1433.
149. Abbas, M.; Ali, A.; Arshad, M.; Atta, A.; Mehmood, Z.; Tahir, I.M.; Iqbal, M. Mutagenicity, cytotoxic and antioxidant activities of Ricinus communis different parts. *Chem Cent J* **2018**, *12*, 3.
150. Erhabor, J.O.; Idu, M. In vitro antibacterial, antioxidant, cytogenotoxic and nutritional value of Aloe barbadensis Mill.(Asphodelaceae). **2020**.